DISSERTATION

ANTICIPATED PERFORMANCE OF $Cu(In,Ga)Se_2$ SOLAR CELLS IN THE THIN-FILM LIMIT

Submitted by

Ana Kanevce

Department of Physics

In partial fulfillment of the requirements

For the Degree of Doctor of Philosophy

Colorado State University

Fort Collins, Colorado

Fall 2007

COLORADO STATE UNIVERSITY

July 17, 2007

WE HEREBY RECOMMEND THAT THE DISSERTATION PREPARED UNDER OUR SUPERVISION BY ANA KANEVCE ENTITLED 'ANTICIPATED PERFORMANCE OF $Cu(In,Ga)Se_2$ SOLAR CELLS IN THE THIN-FILM LIMIT' BE ACCEPTED AS FULFILLING IN PART REQUIREMENTS FOR THE DEGREE OF DOCTOR OF PHILOSOPHY.

Committee on Graduate Work

Professor M. Gelfand

Professor R. G. Leisure

Professor C. S. Menoni

Adviser Professor J. R. Sites

Department Head Professor D. H. Hochheimer

ABSTRACT OF DISSERTATION

ANTICIPATED PERFORMANCE OF $Cu(In,Ga)Se_2$ SOLAR CELLS IN THE THIN-FILM LIMIT

The demand for alternative sources of energy is rapidly increasing. Although thin-film polycrystalline solar cells are an excellent candidate for clean energy production with competitive prices, the knowledge of device physics is still incomplete, especially in the very low thickness limit. The goal of this work is to enhance the understanding of thin-film solar cells with submicron absorbers, which would lead to significantly lower production cost and wider commercial usage. One of the largest obstacles towards increased large scale $Cu(In,Ga)Se_2$ (CIGS) production is the expense of the elements involved, especially indium. The usage of In and the other materials, as well as the deposition time, can be significantly decreased, if the thickness could be reduced without significant efficiency loss. The main focus of this work is on CIGS cells with thin absorbers, in particular: (1) the influence of specific parameter variations on device performance, (2) the sensitivity to nonuniformities in key parameters, (3) the possibility for illumination from both sides of the cell, and (4) the role of the buffer layer between absorber and contact.

As the cells become thinner, the distance between the back contact and the electric-field region narrows, or, for very thin cells, completely disappears. One of the main differences between thick and thin cells is that in thinner cells more light reaches the back-contact and back-contact recombination becomes a significant loss mechanism. A choice of the back-contact material or increased fraction of Ga towards the back are

needed to avoid losses. The Ga/In ratio needed and the effect of Ga distribution through the absorber on the performance of ultra-thin cells are analyzed, and compared with the thick cells.

In addition to the issues with uniform thin absorbers, there is a concern of increased sensitivity to nonuniformities. Fluctuations in the defect density, band gap, thickness or doping affect the voltage. The low voltage area then influences the nonuniform cell performance depending on the voltage difference between the "strong" and "weak" area, the ratio between the "weak" and "strong" area and the distribution of the "weak" area. Thinner cells are more sensitive to thickness nonuniformities, and therefore deposition methods that produce smooth absorbers are desirable for thin devices.

In ultra-thin cells illumination from the back side, i.e. light entering CIGS from the opposite side of the junction, can yield a significant output performance. If certain optimization steps are taken, the back side performance can approach that of the front side. In the case of a back-illuminated cell, the carrier generation occurs in the bulk, making it critical to lower back-contact recombination, as well as to provide good collection. Different parameters such as thickness, doping, minority carrier lifetime and band-gap have an impact on the back illumination performance. The main optimization steps need to be directed towards short circuit current increase. In ultra-thin limit, back- and front illumination performances converge.

Illumination with only low energy photons in cells with the commonly used CdS buffer layer causes distortion in the current-voltage curves, whose mechanism is explained in this work. The difference in distortion for thin and thick devices is studied.

Some alternatives to CdS have a great potential. CdZnS is a higher band gap candidate for buffer layer that has achieved efficiency close to the record one and with some optimization can open the door to efficiencies higher than 20 %.

Ana Kanevce
Physics Department
Colorado State University
Fort Collins, CO 80523
Fall 2007

ACKNOLEDGEMENTS

I am very thankful to Svetlana, Vladimir, and Ivo Kanevce for their infinite love and support. For holding a light to show me the road. For helping me follow my dreams, even if they meant a large distance between us. I would not have come all this way if I didn't have such a great family.

To my advisor, Jim Sites, for giving me the opportunity to become a part of this exciting field. I have inherited an incredible amount of knowledge from him and have been encouraged from start to finish.

The National Renewable Energy Laboratory for funding my work. To Falah Hassoon and Raghu Bhattacharya from NREL for good collaboration and providing cells.

I have appreciated the collaboration with the present and previous students in the Photovoltaic group: Alex Pudov, Caroline Corwine, Jun Pan, Tim Nagle, Alan Davies, Galymzhan Koyshiev , and especially Markus Gloeckler and Samuel Demtsu for many fruitful discussions.

To my committee members Martin Gelfand, Robert Leisure, and Carmen Menoni for serving on the committee and for the review of this manuscript.

To Steve Fonash and his coworkers from Pennsylvania State University for providing AMPS-1D software and to Mark Burgelman and his colleges from the University of Gent, Belguim for providing SCAPS-1D software.

To the employees of the Physics Department at the Unverzitet Sv Kiril i Metodij in Skopje. Especially to Prof. Mirjana Jonoska who shared her passion for physics and who was a real mentor and friend all these years, and to Ane Tuntev, a great physicist and friend.

These years would have been much harder without some good friends standing by my side. Thank you, Sangita. Thank you, Seema. Thank you, Gabriela. Thank you, Christina.

And finally, I am very thankful to my husband, Predrag Šerbedžija, for dealing with me when I've been extremely irrational and difficult. For believing in me, encouraging me, and for making the days wonderful.

CONTENTS

LIST OF FIGURES:

CHAPTER 1

MOTIVATION FOR PHOTOVOLTAIC RESEARCH

1.1. Need for alternative sources of energy

Humans' desire to provide themselves with a more convenient lifestyle is very old and is intricately tied to increased energy expenditures. Environmental awareness and impact on ecosystems as a result of ever increasing energy demands is, however, a much newer phenomenon.

World-wide energy usage in 2005 averaged 12 TW. One quarter of the total energy used in the world was consumed in the US alone, and 85% of that energy depended on fossil fuels (coal, oil, and natural gas) [1]. The energy demands have kept on increasing very quickly, and the consumption will increase even faster with the population growth and the development of underdeveloped regions. The predicted

energy consumption for 2050 will amount to as much as 30 TW. The question arises how to supply all that energy.

Certainly, the straightforward answer is to burn more fossil fuels.

Is that really a choice?

Fossil fuels emit many gases that pollute the atmosphere. Sulfur dioxide and nitrous oxide (main causes of acid rains and smog) are two examples. Our convenient lifestyle also results in a daily output of 16 million tons of CO_2 into the atmosphere [2]. This large CO_2 emission is a primary cause for global warming, and the primary reason for the recent climate changes. Another problem is that oil is not a renewable resource. Its supply will eventually be depleted. There are different estimates for predicting how fast we will run out of oil, ranging between 10 years and over a century. Oil is spent million times faster than it is formed [2], and most reports agree that complete depletion is unavoidable. Additionally, the heterogeneous distribution of world-wide oil reserves has been observed to generate political and economical tensions, which may be expected to increase in the future as oil reserves run low.

Even if the amount of available fossil fuels were infinite, the damage that burning fuel is doing to the environment is irreparable and unforgivable. Clean and renewable sources of energy are a sound alternative. Here, the focus will be on solar energy, one of the most promising sources of alternative energy.

1.2. Potential of solar energy

The power of sunlight incident on the Earth is 125,000 TW [3]. That is 10,000 times more than what we currently use, and the sun will be available for a very long time for all of us. Energy from the sun makes the life on this planet possible. Why not take greater advantage of it?

One way to utilize the energy of the sun is by converting it into electrical energy. Solar cells perform this conversion based on the photovoltaic effect, first reported in 1839 by Becquerel.

Although the idea of converting light energy into useful electricity dates back to the 19th century, the era of the modern solar cells starts in the 1950's at Bell labs where the first 6%-efficient silicon solar cell was produced by Chapin *et. al* [4]. The first efforts for development of photovoltaic (PV) devices were directed towards space applications, and solar cells are still today the main source of power in space. PV use was expanded to terrestrial applications about three decades ago, and it keeps on growing rapidly. That growth is inspired by many advantages of solar cells, the primary one being its low impact on the environment. Another very important advantage is the more or less homogenous distribution of solar energy on the Earth, making it accessible to everyone, anywhere.

The portability of solar modules makes them commercially attractive now for remote areas. The number of villages in the world not connected to an electrical grid is estimated to be two million [2]. One third of the world's population lives in these villages. Extending the electricity grids to remote rural areas, which are scattered and

usually have lower energy demands compared to the cities, is often considered financially unattractive for the electricity providing companies. Basic electricity needs for agriculture, education, heating, and light in these areas are usually satisfied with electrical sources such as rechargeable batteries and small fossil fuel generators [5]. These sources are very often expensive and unreliable. It is easy to envision the impact this lack of power has on the development and standard of living in these areas. Providing solar-powered electricity to remote areas may be one of very few ecologically and commercially acceptable solutions.

Even though PV usage has clear advantages over conventional energy sources there are obstacles to its wider use. The main reason is that it is about three times higher in cost. In order to lower the PV price and expand its usage, steps need to be taken to lower the quantity of materials and the energy used to manufacture solar cells.

1.3. Thin-film polycrystalline cells

Today, the majority of solar cells are made of crystalline silicon. Silicon produces devices with highest efficiency (24.5% [6]) that are also very stable. Silicon's availability is huge, but crystalline Si cells require an expensive production process. Silicon is fragile, and it is an indirect band-gap material. Both of these features require production of relatively thick cells. A typical Si-cell thickness is approximately 300 μm, more than 100 times the thickness of a typical polycrystalline thin-film cell.

Although not commercially established as well as Si, thin-film polycrystalline solar cells, such as CdTe and CIGS, have a great advantage of significantly lower production cost. Lower cost comes not only from lesser semiconductor material usage,

but also from lower deposition temperatures (by ~1000°C) and from higher forgiveness towards nonuniformities, which allows usage of less pure materials. Even though thin-film cells have obvious advantages, still 90% [7] of the world-wide PV market belongs to silicon. In the US, however, the production of silicon and thin-film solar cells in 2006 was roughly equal. The progress towards higher thin-film efficiency and production growth has been tightly connected with the understanding of the materials and devices.

1.3.1. $Cu(In,Ga)Se_2$ cells

$Cu(In,Ga)Se_2$ (CIGS) is a very promising photovoltaic material, with conversion efficiencies approaching the 20% milestone. The highest efficiency CIGS cell (19.5%) was produced in the National Renewable Energy Laboratory in 2005 [8] with a CdS buffer layer, and somewhat later a 19.52% efficient cell with CdZnS buffer layer [9]. These are the highest efficiency thin-film solar cells to date. In addition to high conversion efficiencies, CIGS cells have proved good outdoor stability. Together with the optimistic prognoses for CIGS cells future development, several problems arise that need to be addressed. One of the biggest concerns is the price and availability of the materials involved.

1.3.2. Material usage

The availability and price of the element indium is threatening to become a bottleneck to larger scale CIGS production. Indium is produced as a byproduct of Zn mining. To meet a relatively modest goal of 20 GW power production by 2050, In

production would need to increase by 60%. In a more optimistic scenario of 100 GW production by that date, without changing the production method, the supply of In becomes a significant problem [10]. Minimizing In usage in PV cells is one very important concern. Some ways to handle this problem are replacement of In with other group 3 materials such as Ga and Al, production of devices with thinner absorbers, and increases in production yield. Partial substitution of In with 30% Ga improves the performance, but more Ga introduces additional defects [11] that to date have been detrimental for the devices. Solar cells with Al substituted for Ga, $Cu(In,Al)Se_2$ have achieved efficiencies inferior to the ones with Ga [7, 12].

1.3.3. Ultra-thin absorbers

Clearly one of the main goals of today's PV research is using less semiconductor material by making the cells thinner [7, 12]. Thinning will not only save material, but will also lower production time, and the energy needed to produce the solar cell. All of these factors will decrease the production cost.

CIGS has a high optical absorption coefficient. It can therefore absorb most of the incident photons within 1 μm of absorber thickness, which makes it suitable for an ultra-thin operation. Several research groups have tried to produce thin absorbers with minimal efficiency loss. A review of ultra-thin absorber parameters produced in different labs will be given in Chapter 4. The present work will provide analyses of several aspects of thin cells.

CHAPTER 2

BACKGROUND

2.1. Solar spectrum

The radiation spectrum of the Sun can be approximated by a black-body with a temperature of approximately 6000 K and can therefore be well described with Planck's radiation law. The intensity and spectral distribution that arrives on the Earth's surface is significantly altered due to atmospheric scattering and absorption. The radiant power per unit area is strongly dependent on the path length of Sun's rays through the Earth's atmosphere. The term air mass intensity (AM) is often used to denote the ratio of the optical path to a normal path at sea level on a cloudless day hence:

$$AMx = \frac{1}{\cos\theta}\ , \qquad (2.1)$$

Where $\theta = 0$ corresponds to perpendicular incidence of the beam.

The standard terrestrial spectrum used in photovoltaic research is approximately AM 1.5 [13, 14] and is shown in Fig. 2.1.

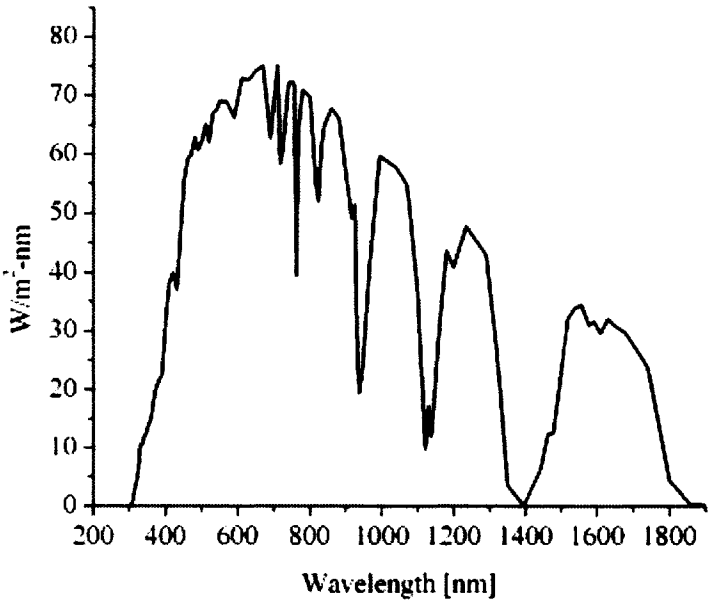

Figure 2.1. AM 1.5 terrestrial solar spectrum

2.2. Solar cell background basics

A solar cell is a semiconductor diode that converts sunlight into electricity based on the photovoltaic effect. This section briefly reviews the basic principles of solar cell operation. Detailed reviews of semiconductor properties can be found in Refs. [14] and [15], for example.

2.2.1. Semiconductors

All of the valence electrons in semiconductors at T = 0 K are weakly bonded to their atoms. They are in the valence band, can not move around freely, and the semiconductor does not conduct electricity. A small forbidden energy gap (the order of one eV) separates the valence band from the conduction band. At higher temperature, due to thermal excitation, some electrons gain enough energy to break the bond with their atom, and move to the conduction band. Excited electrons leave a positively charged empty space – a hole in the valence band. The electrons and holes can carry charge, and the semiconductor now is conducting. The conductivity properties can be significantly altered by substituting atoms with a different valence from the rest of the material – doping. Such doping generally introduces additional energy levels within the forbidden band, and thereby increases the semiconductor conductivity. Doping can be either p-type (the majority of charge carriers are holes in the valence band) or n-type (the majority carriers are electrons in the conduction band).

When light with photon-energy higher than the band gap is incident on the material, it generates additional electron-hole pairs. These extra generated carriers will recombine at the same rate at which they are generated, unless they are separated by a force-field. Solar cells are produced by joining together p-type and n-type material into a p-n diode. The junction between the p- and the n- semiconductor can be a homojunction, made by doping two portions of the same material (for example silicon) with different type dopands. Alternatively, the junction can be a heterojunction, when the n-type and p-type semiconductors are different materials.

Once in contact, electrons flow from the n-type to the p-type material, and holes from p to n, leaving ionized atoms behind. These ions create an electric field in the direction opposite to the carrier diffusion that opposes the further diffusion. The same electric field separates light-generated electrons and holes and directs them towards metal contacts on each side of the diode.

If a load is connected to the contacts, a current will flow through it. The basic transport equations governing the flow will be discussed in Chapter 3.

2.2.2. Requirements from a solar cell material

The number of materials which exhibit the photovoltaic effect and can be used for solar cell production is large. To be useful for practical PV applications, however, the device needs to satisfy numerous requirements.

The first requirement is to efficiently convert solar energy into electricity. Second, the material used needs to be inexpensive, available in large quantities and non-toxic. Third, the device production method should be inexpensive, fast, simple and environmentally benign. Fourth, the device performance should be stable for extended periods of time.

2.3. $CuInSe_2$ solar cells

2.3.1. $Cu(In,Ga)Se_2$ cells structure

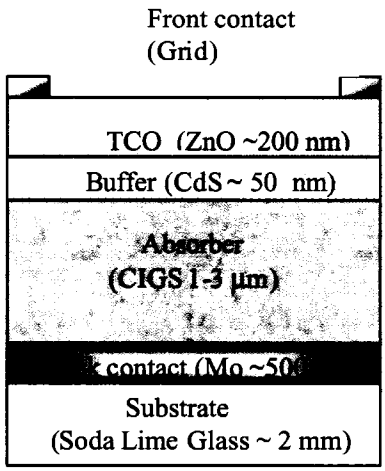

Figure 2.2. A schematic of a typical CIGS solar cell

A schematic of a typical CIGS solar cell is shown in Fig. 2.2. Light enters the cell through the transparent conductive oxide layer (TCO), passes through the CdS buffer layer, and enters the absorber. The p-n junction is formed by p- type CIGS layer and n-type buffer layer.

The semiconductor materials are deposited on a substrate. The most commonly used substrate is soda-lime glass, which has a low price and good thermal expansion coefficient match with CIGS. In addition, sodium from such a substrate diffuses into CIGS and has beneficial effects. It replaces substitution defects where a Cu atom is replaced with In (In_{Cu}) that act as compensating donors. It also catalyzes the dissociation of molecular oxygen. Oxygen atoms passivate selenium vacancies V_{Se} on the grain boundaries, which would otherwise act as recombination centers.

CIGS devices have also successfully been deposited on flexible substrates, such as plastic or metal foils. Although devices with these substrates do not obtain the same efficiencies as the glass substrate ones, they extend the application possibilities.

2.3.2. Absorber layer

The absorber layer is the most important layer in the PV device. $CuInSe_2$ (CIS) is a I-III-VI compound with a chalcopyrite structure. It is a direct band-gap semiconductor material and has a large absorption coefficient ($\alpha \sim 10^5$ cm^{-1}). Most of the incident sunlight is absorbed close to the p-n junction. As a result, the cells based on CIS can be made thin and with low cost.

To produce efficient devices, it is important to match the band-gap of the absorber layer to the solar spectrum. The ideal band-gap for the solar spectrum is 1.4 eV [16]. CIS has a lower-than-optimal band gap of 1.02 eV, and, because of that, the best CIS cells have achieved efficiencies of 15%.

The band-gap can be increased by partial substitution of the In cation with other group III elements such as Al or Ga, or by replacement of Se with S. The record device [8] was produced with a 30% In substitution with Ga. This device had a band gap of 1.15 eV and an efficiency of 19.5%.

The electrical properties of CIGS depend very strongly on the stochiometry [17]. Doping of CIGS comes from native defects, mainly from V_{Cu} (copper vacancies) that act as shallow acceptors.

2.3.3. Buffer layer

CIGS solar cells with a buffer layer generally have superior characteristics compared to those without. Such a layer can provide good junction formation, lower interface recombination, and decrease leakage. Cells containing CdS have been most efficient for a long time, but CdS introduces current loss at wavelengths below 520 nm (corresponding to photon energies above the CdS band gap). There have been many attempts to substitute CdS with an alternative buffer layer. A thorough review of alternatives is given in Ref. [18]. However, until recently, all of the devices with alternative buffer layers performed inferior to the ones with CdS, although ZnS(O,OH) was close when deposited on the same substrate. Recently, a cell with CdZnS buffer was produced [9] having same efficiency as the record CdS/CIGS cell and a potential to surpass it.

2.3.4. Back contact

The back-contact material is a metal on the bottom of the absorber whose role is to collect the carriers from the absorber and deliver them to the external load. In standard thickness cells, the requirements for back-contact material are to have low resistivity, not to impede the flow of majority carriers, holes, and, in CIGS cells, to allow diffusion of Na from the substrate to the semiconductor. So far, the best cells have been produced with molybdenum as a back contact. The back-contact material becomes more important and more interesting as the cells become thinner, because the carrier generation profile shifts closer to it.

2.3.5. Window layer

The ZnO layer is referred to as a "window layer" or a transparent conductive oxide (TCO). For most photons to be absorbed by CIGS, it is very important for the TCO to have a large band gap (3.3 eV) and therefore to be transparent for most of the solar spectrum. Usually an antireflective coating is deposited on the top of the cell to minimize the reflection losses.

2.3.6. p-n junction

The p-n junction in a typical CIGS cell is formed between the p-type CIGS and n-type CdS. The energy band diagram for such a cell is shown in Fig. 2.3. The CIGS band gap is 1.15 eV and its thickness is 1 μm. The difference in electron affinities between CIGS and CdS results in a band-gap discontinuity. The conduction-band offset ΔE_c between CIGS and CdS is positive by convention, meaning that CdS conduction-band minimum is higher than that of CIGS. Wei and Zunger [19] calculated the theoretical valence-band offset between CdS and CIGS. The conduction-band offset for 1.15 eV CIGS can be deducted from their calculations to be $\Delta E_c = 0.3$ eV, a value within the optimal range. An offset larger than 0.5 eV creates a strong barrier for light-generated electrons, thus limiting the current transport. Zero or negative conduction-band offset allows interface recombination, limiting voltage.

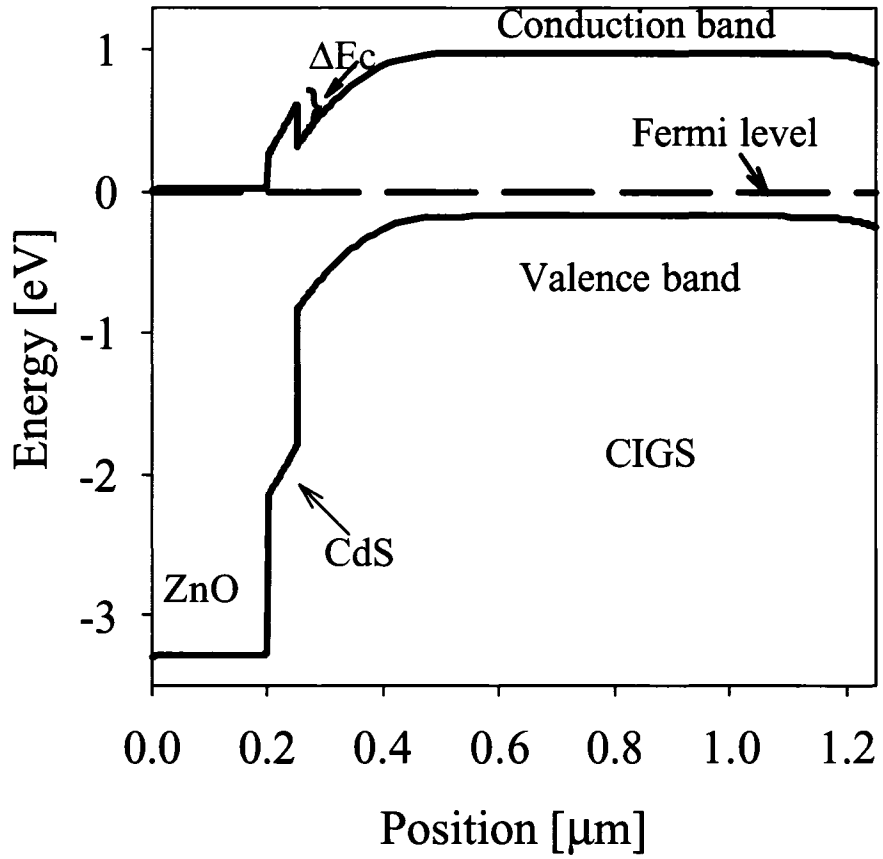

Figure 2.3. A simulated band diagram of a typical CIGS solar cell

CHAPTER 3

METHODS

3.1. Characterization techniques

Characterization of solar-cell devices is necessary to determine the sources of losses and suggest ways to minimize them. Three characterization techniques are used in this research: current-voltage (J-V), quantum efficiency (QE) and capacitance-voltage (C-V).

3.1.1. Current –voltage characteristics

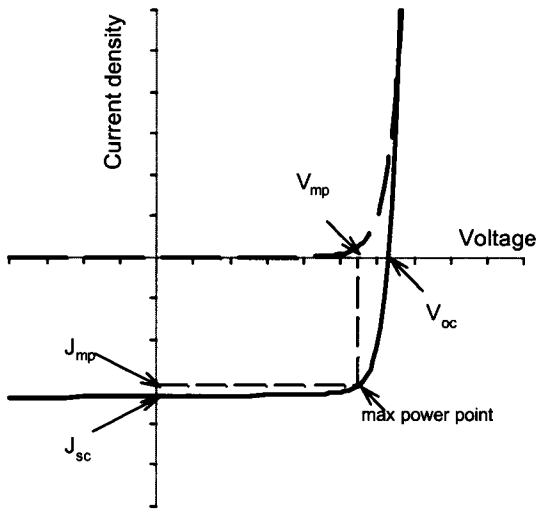

Figure 3.1. Current-voltage curve of a solar cell in dark (dashed) and in light (solid).

The most common way to describe the performance of a solar cell is with its current-voltage characteristics. The current-voltage curve of an ideal solar cell in the dark follows the exponential diode law (long-dash line in Fig. 3.1). When the cell is illuminated, the curve is shifted downwards by an amount referred to as the light-generated current J_L, which in ideal case is independent of voltage and the same as the short-circuit current J_{sc}.

$$J = J_D - J_L = J_0 \exp\left[\frac{qV}{AkT} - 1\right] - J_L \qquad (3.1)$$

Here, J_0 is the diode saturation current, A is diode quality factor (equal to 1 in the ideal case), q is elemental charge, k is Boltzman constant, and T is temperature.

Conversion efficiency is generally the parameter of most interest for solar cell applications. It is often broken down into three different parameters: 1) Short-circuit current density J_{sc} *[1], 2) open-circuit voltage V_{oc}, and 3) fill-factor (FF).

The short-circuit current, i.e. the current at V = 0, depends on the number of photo-generated carriers and their collection efficiency. The number of generated carriers can be maximized by minimizing the area taken by contact grids and by sufficiently thick absorbers, which allow all of the photons with sufficient energy to be absorbed. Collection efficiency depends on the recombination mechanisms. The losses in short-circuit current can be analyzed from the quantum efficiency curves (Chapter 3.1.2).

Open-circuit voltage is the voltage at zero current, when the forward current balances the photogenerated current. The open-circuit voltage is equal to the difference in quasi-Fermi levels for electrons and holes between the two sides of the device, and its maximum is determined by the absorber band-gap E_g. From the diode equation, V_{oc} is equal to:

$$V_{oc} = \frac{AkT}{q} \ln\left(\frac{J_L}{J_0} + 1\right) \qquad (3.2)$$

The saturation current J_0 depends on the material properties and the cell structure and is limited by recombination coming from several different recombination mechanisms: recombination in the bulk CIGS, in the space-charge region, and at the CdS/CIGS interface.

The power extracted from the cell is a product of current and voltage. At some point on the current-voltage curve (i.e. for a specific load) this product has a maximum

[1] The current density will be referred to as current throughout the text

value. That point is maximum-power point, and the corresponding current and voltage are referred to as the maximum-power current J_{mp} and the maximum-power voltage V_{mp} (Figure 3.1).

In addition to V_{oc} and J_{sc}, the maximum power depends on how "square" the curve is. The "squareness" is defined by fill factor (FF):

$$FF = \frac{V_{mp} J_{mp}}{V_{oc} J_{sc}} \tag{3.3}$$

Finally, the efficiency involves all these three parameters and can be calculated as:

$$\eta = \frac{P_{out}}{P_{in}} = \frac{J_{sc} V_{oc} FF}{P_{in}} \tag{3.4}$$

P_{in} is the incident light power on the cell. It is commonly taken to be 100 mW/cm^2 for standard solar illumination. This illumination is referred to as AM 1.5 illumination, and it is equivalent to sunlight passing through 1.5 times the air mass of vertical illumination.

Equation (3.1) is the ideal diode equation, but real solar cells have additional losses, such as series resistance and leakage or shunt conductance. The series resistance R_s comes from the resistance in the bulk of the semiconductor and the contact resistances. Shunt resistance R_{sh} can represent any parallel paths for current flow. An equivalent circuit of a solar cell with these parasitic resistances is shown in Fig. 3.2.

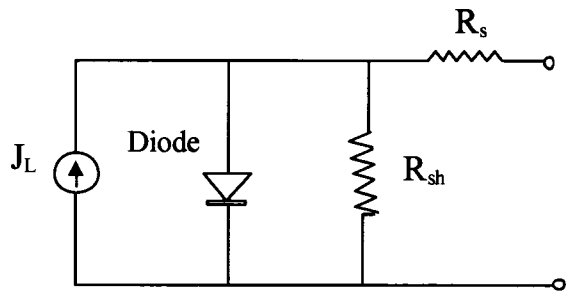

Figure 3.2. An equivalent circuit of a solar cell

The p-n junction is represented by a diode and the photoexcitation by a current source J_L in parallel with the diode. When series and shunt resistance are incorporated into the diode equation, it becomes:

$$J = J_D - J_L = J_0 \exp\left[\frac{q}{AkT}(V - R_S J)\right] + \frac{V - R_s J}{R_{sh}} - J_L \qquad (3.5)$$

Here R_s is the series resistance and R_{sh} is shunt resistance.

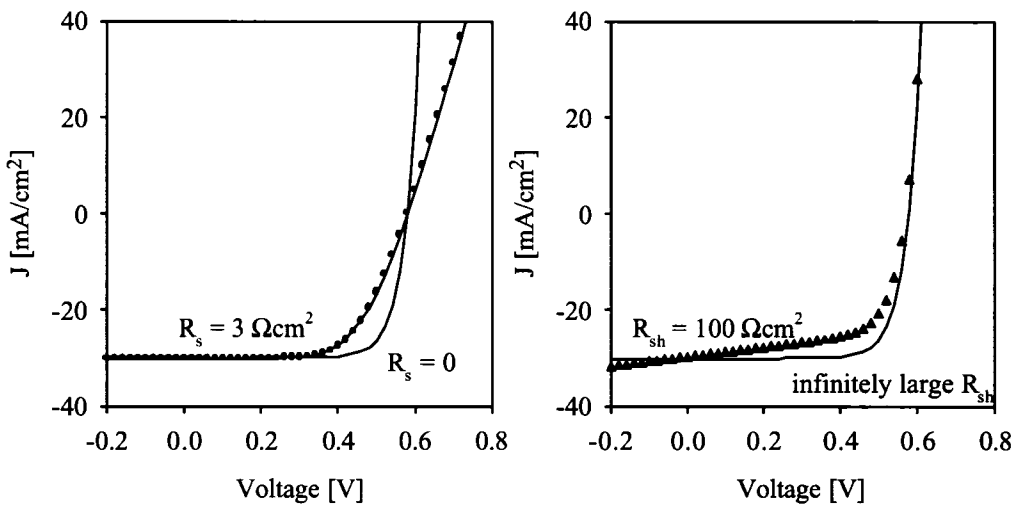

Figure 3.3. Simulated current-voltage curves without parasitic resistances (lines) with nonnegligible series resistance (circles) and finite shunt resistance (triangles).

The effect of non-zero series resistance and non-infinite shunt resistance on current-voltage curve is shown in Fig. 3.3. Both of the parasitic loses reduce the fill factor, but in extreme cases, they can also reduce the J_{sc} and V_{oc}.

Current-voltage measurement with more detailed analysis can help in understanding the solar cells losses further. The shunt conductance can be extracted from the dependence of the derivative dJ/dV on voltage, and diode quality factor and series resistance (if the shunt resistance is high) from a dV/dJ vs. $1/(J+J_L)$ plot. A more detailed analysis of current-voltage curves is given in Ref. [20].

3.1.2. Quantum efficiency

Quantum efficiency (QE) is defined as a ratio of collected carriers to photons incident on a device at each wavelength. In the ideal case, every photon creates an electron-hole pair which contributes one carrier to the photocurrent, and the quantum efficiency is 100% for photon energies above the band gap, and zero below. In real cells, that is never the case. Regardless of efforts to minimize reflection loss, some light is reflected from the front surface of the solar cell. The first step in QE loss analysis is to correct for reflection loss. The corrected QE curve can be referred to as the internal QE.

Since the photon penetration into a solar cell is very dependant on photon energy, the QE curve can help localizing the most important current losses for each particular device (Fig. 3.4). Photons with energies lower than the band-gap do not contribute to the current; therefore the long wavelength cut-off of the quantum efficiency curve can be used to estimate the absorber band gap. Short wavelength losses are result of the

absorption in the CdS ($\lambda < 520$ nm) layer and the TCO ($\lambda < 375$ nm) layer, because the photons generated in these layers generally do not get collected.

The photons with energies slightly higher than the band gap will penetrate deepest. The negative slope in the quantum efficiency curve in the high wavelength region is due to their incomplete collection.

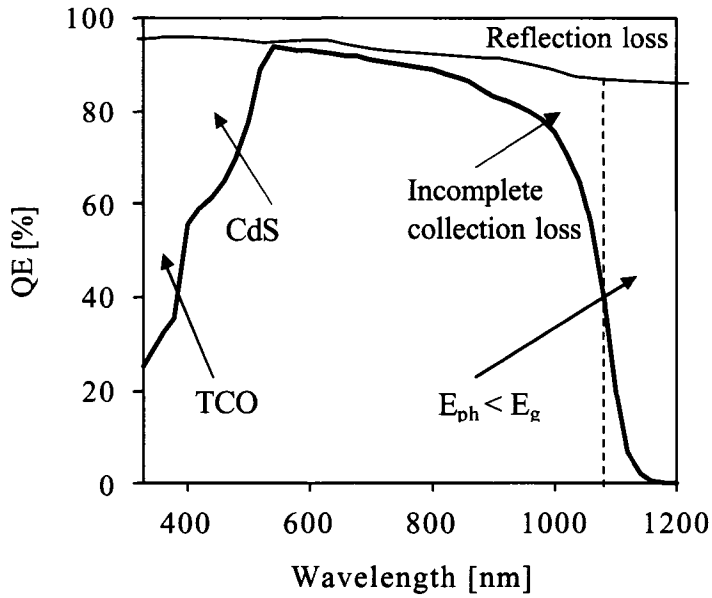

Figure 3.4. A simulated quantum efficiency curve with extraction of current losses

The photocurrent can be obtained by integrating the product of the appropriate illumination spectrum, assumed here to be AM 1.5, and the quantum efficiency:

$$J_L = q\int AM_{1.5}(\lambda)QE(\lambda)d\lambda \qquad (3.6)$$

Integration within a certain wavelength range can determine the fraction of photocurrent lost due to a specific loss mechanism. For example, integration between band gap energies of TCO (3.3 eV) and CdS (2.4 eV) yields the current loss due to absorption in CdS.

3.1.3. Capacitance-voltage

Common goals of capacitance measurements are to determine the space-charge region width and the carrier density in the absorber.

In an ideal diode, with an abrupt delineation of the depletion region, the junction can be viewed as a parallel plate capacitor with distance between plates equal to the depletion-region width W [21]. The capacitance of this capacitor is:

$$C = \frac{\varepsilon A}{W} \tag{3.7}$$

where ε is dielectric constant, and A is the area.

Variation of applied voltage affects the capacitance by changing the charge at the edges of the depletion region. The capacitance- voltage relation can be used to determine the depletion width as well as the carrier density in the less doped semiconductor. In CIGS cells, the hole density in the absorber is generally at least an order of magnitude lower than the electron density in illuminated CdS, and thus capacitance measurements determine the hole density in the absorber. The C^{-2} vs. V dependence is linear, with slope inversely proportional to the doping:

$$\frac{A^2}{C^2} = \frac{2}{q\varepsilon N}(V_{bi} - V) \tag{3.8}$$

here N is the doping density, V_{bi} is the built in potential and V is the applied voltage.

Guidelines for capacitance measurement interpretation for polycrystalline and nonideal cells are given in Ref. [22].

3.2. Numerical modeling

3.2.1. Introduction / Why using modeling techniques?

A model is a theoretical construction created to represent real processes and parameters that influence them. Models are widely used in science to simplify complicated systems, by neglecting the non-crucial features. Distinguishing between important and non-important features or parameters becomes the most important task for the modeler. A good model, where all the important parameters are taken into account and the nonimportant ones are omitted, is a good presentation of a real phenomenon and leads to its enhanced understanding.

Modeling is widely used in analysis of single-crystal solar cells. Due to the complex nature of thin-film polycrystalline solar cells, the need for numerical modeling methods is higher.

Numerical modeling techniques can help the understanding of solar cells, and should give the manufacturers additional ideas of how to vary their production methods to improve the product performance. A schematic is given in Fig. 3.5. Once the cell is produced, it needs to be characterized to determine the losses. Analysis of characterization curves leads to hypothesis of where these losses come from. Modeling techniques can often support the hypothesis, and provide physical explanation of the mechanism behind the loss. Numerical modeling may predict the quantitative impact of changes in material properties on device performance and suggest ways to change the deposition process and improve the performance.

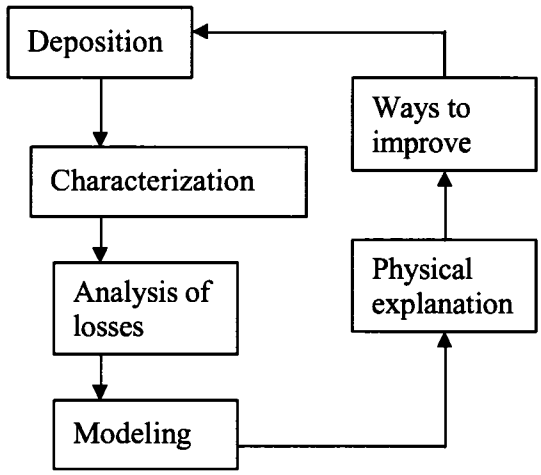

Figure 3.5. A schematic of the modeling role in improvement of solar cells

3.2.2. How much can we trust modeling results?

Although it is clear that modeling can be a valuable tool for thin-film solar-cells improvement, interpretation of modeling results requires extreme caution. Modeling is only useful if it describes reality, and if not compared with experimental data it can easily lead to erroneous conclusions.

The number of parameters that can be varied in the particular solar-cell model is larger than 50 [23]. Obviously, a problem with 50 variables is too ambiguous to solve reliably. It is therefore necessary to minimize the number of variable parameters by fixing many of them at "reasonable" values. It is challenge to choose the appropriate parameters. Many of them depend on deposition methods and can thus vary between devices. Due to the high number of variable parameters, different sets of parameters can lead to similar output performance curves. Therefore, drawing conclusions through a fit of a single set of experimental data can be misleading. To use simulations for explaining

experimentally observed behavior, more complete sets of experimental data and knowledge of as many of the material properties as possible are necessary.

3.2.3. AMPS-1D and SCAPS-1D

Several software programs have been written with a specific purpose of modeling solar cells. They have different possibilities and limitations, but the basic principles are the same. A review of different simulation methods and their advantages and disadvantages is given in Ref. [23]. Two of them have been used for calculations in this work. They are: Analysis for Microelectronic and Photonic Structures (AMPS-1D), developed by S. Fonash and colleagues at Pennsylvania State University, and Solar Cell Capacitance Simulator in 1 Dimension (SCAPS-1D) developed by M. Burgelman and colleagues at the University of Gent, Belgium [24, 25].

One advantage of SCAPS-1D over AMPS-1D is its possibility to calculate capacitance-voltage and capacitance-frequency characteristics. Another advantage is inclusion of interfaces between layers. AMPS-1D, on the other hand, has been more stable, it has better plotting facilities, and it can run multiple simulations simultaneously.

3.2.3.1. Basic concepts

Since AMPS-1D was mostly used in this work, its principles will be explained in more details. It solves numerically three coupled partial differential equations: the Poisson equation and the continuity equations for electrons and holes as a function of position x.

The Poisson equation connects the electric potential and the charge:

$$\frac{\partial}{\partial x}\left(-\varepsilon(x)\cdot\frac{\partial\Phi(x)}{\partial x}\right)=q\left(p(x)-n(x)+N_D^{+}(x)-N_A^{-}(x)+p_t(x)-n_t(x)\right) \qquad (3.9)$$

where p is free hole density, n is free electron density, N_D^+ is ionized-donor density, N_A^- is ionized-acceptor density, $n_t(x)$ and $p_t(x)$ are trapped electron density and trapped hole density, respectively, and ε is dielectric constant.

The continuity equation for electrons is

$$\frac{1}{q}\left(\frac{dJ_n}{dx}\right)=-G(x)+R(x), \qquad (3.10)$$

and for holes:

$$\frac{1}{q}\left(\frac{dJ_p}{dx}\right)=G(x)-R(x), \qquad (3.11)$$

where J_n and J_p are the electron current and hole current, respectively. G(x) is the generation rate, and R(x) is the recombination rate, which generally involves band-to-band recombination and SRH recombination and is nonlinear in n and p.

The illumination intensity decreases exponentially with penetration into the solar cell. The generation rate is proportional to the remaining illumination, and the exponent contains the wavelength-dependent absorption coefficient of the particular layer:

$$G(x)=-\frac{dI(x)}{dx}=\alpha I(x_0)\exp\left(-\alpha(x-x_0)\right) \qquad (3.12)$$

where I(x) is the illumination intensity at the position x, x_0 is the point at the beginning of the particular layer. The unknown variables in a solar cell simulation are the electrical potential Φ and the carrier concentrations p and n, or alternatively, the potential and the quasi-Fermi levels for electrons and holes (Φ, E_{Fn} and E_{Fp}).

To set up a numerical simulation to model a solar cell, the cell is divided into N segments, separated by N+1 grid points. Boundary conditions are applied at the ends, and the set of 3(N+1) unknowns is determined for each grid point by iteration using Newton-Raphson method [26].

3.2.3.2. CIGS cell parameters used

Ref. [27] gives a good starting point for assignment of baseline parameter values, or for reasonable ranges of variation. Some of the parameters choices are explained below.

The diffusion length of minority carriers determines how far the electrons can diffuse before they recombine with the majority holes and therefore will very strongly affect the device performance. It is given by:

$$L_n = \sqrt{D_n \cdot \tau_n} \tag{3.13}$$

where D_n is diffusion constant, and τ_n is electron lifetime. The electron lifetime is very sensitive to variety of recombination mechanisms. The baseline value used for CIGS is 1.6 ns, slightly lower than that in Ref. [27]. This work mainly deals with cells thinner than 1 micron, which may well have higher defect density than the 'standard thickness' [2] ones discussed in Ref. [27].

The diffusion constant D is related to the carrier mobility μ by the Einstein equation:

$$D = \frac{kT}{q}\mu \tag{3.14}$$

[2] Standard thickness of CIGS cells is 2-3 μm

The electron mobilities in single crystal CIGS have reported values ranging between 90 and 900 V/cm^2-s [7]. The electron mobility value used here is 100 V/cm^2-s, since polycrystalline materials are expected to have lower mobilites than the single crystalline ones.

The absorption spectrum for CIGS with a band gap of 1.15 eV has been measured by Paulson *et. al.* [28]. This spectrum with minor adjustment is given in Ref. [29]. The absorption edge is shifted for different band gaps.

Widening of the band gap by increasing the Ga content can also increase the defect density in the materials [11]. This effect has not been taken into account in Ref. [27], but its addition was necessary for an agreement with the experimental data. For Ga content lower than 60%, this additional defects impact on the device performance is assumed to be negligible. However, for higher Ga/(In+Ga) the defect density increase is observed to affect the device parameters stronger. The relation of defect density as a function of the absorber band gap in the model follows the experimental results in Ref. [11].

The optical reflection at the front solar-cell surface is taken to be 5%. The optical reflection from the back contact is set at 80%, except in Chapter 6, where for back-side illumination the opaque back contact is replaced with a transparent material with 15% reflection.

When cell parameters are allowed to vary as a function of position, they are simulated by introducing multiple layers with gradually changing parameters.

CHAPTER 4

RESULTS: ULTRA-THIN CIGS ABSORBERS

4.1. Results

The results in this thesis are presented in the following four chapters. This chapter presents the device physics of cells with absorbers thinner than 1 micron. It gives a review of sub-micron CIGS devices that have been reported to date, followed by results obtained by numerical simulations.

First, the changes in the cell performance that happen in thin cells are discussed. The effect of parameter variations on cell performance between thin and thick cells is compared. The parameters investigated are hole density in the absorber, minority-carrier lifetime, the increasing importance of the back contact in thin cells, and the conduction-band profile.

Thinner devices are generally more affected than thick ones by fluctuations in some, but not all parameters. The fluctuations in absorber thickness certainly have more impact on thin cells compared to the thick ones. The impact of lateral voltage nonuniformities on the device performance, with an emphasis on submicron cells is examined in Chapter 5. The impact of the weaker (lower voltage) area on the entire device performance is dependant on the difference between the strong vs. weak area voltages, the ratio of the weak vs. total cell area, as well as on the TCO resistance.

Once the cell is thin enough, a nonnegligable percentage of the incident light from the back side can reach the p-n junction. This light might come from simultaneous illumination from both sides, or from light reflected by the back contact in thin cells or from the bottom cell in tandem devices. Ways to optimize the device for illumination from the back, without compromising the front-illumination performance are discussed in Chapter 6.

Chapter 7 reviews the role of the buffer layer in thin CIGS cells. When a CIGS cell is illuminated from the back side, or when it is used as the bottom cell in a tandem structure, high energy photons may not reach the p-n junction. In that case, the current-voltage curve may be seriously distorted [30]. The mechanism for this distortion and its thickness dependence are presented in Chapter 7. Ways to avoid the distortion by varying CdS properties or by substituting another material for CIGS are suggested.

4.2. Thin CIGS review

Motivated by lower material cost and lower production time, several groups have produced devices with thinner absorbers. In a standard device, the absorber thickness is

typically 2 μm. Thickness reduction down to 0.5 μm would (assuming the same yield) save 75% of the semiconductor material and, if the deposition rate is kept unchanged, the deposition time would be four times shorter. Thinning from 1.8 μm to 0.15 μm [31], for example, decreased the deposition time from an hour to only 8 minutes.

The most significant achievements for producing ultra-thin cells, but still with good performance, are shown in Figure 4.1. Devices produced by 3-stage process are marked with open symbols and by codeposition with filled symbols.

Some of the first relatively successful attempts are given in Ref. [32] (1998) (hexagons in Figure 4.1) and Ref. [33] (1997) (diamonds in Figure 4.1). The efficiencies achieved are 13.1% for a 0.86-μm device and 9.9% for a 1-μm device, respectively. Both of these reports show reduction in all J-V parameters as the cells are thinned, and the only attempt for a device with absorber thickness below 0.5 μm is significantly shunted. AFM images in Ref. [32] show a roughness of 0.3-0.4 μm for all thicknesses. This roughness scale is comparable to the thickness of the 0.46 μm device, and therefore the Mo back contact might not be fully covered by CIGS. The same reference shows a decrease in the grain size for thinner absorbers, which is probably the cause of the voltage and fill-factor loss observed for these materials.

More recently, thin absorbers reported in Ref [34] (2003) (triangles in Figure 4.1), Ref. [35] (squares), and the latest ones in Ref. [36] (2006) (marked in Figure 4.1 with circles), have shown significant improvement in voltage and fill-factor. The absorber films of the more recent ultra-thin devices are smoother, making it possible to produce ½-μm or thinner devices. The thinnest device with reasonable performance [34]

is 150 nm thick and 5% efficient. The best 1-μm device [36] has achieved efficiency of 17.1%, which is only 2.4% less than the record CIGS cell.

Submicron absorbers have also been successfully produced with transparent back contacts [37]. Their efficiencies (crosses in Fig. 4.1) fall within the same range as the standard cells with a Mo back contact.

Thin cells, ($d < 0.5$ μm), and especially the thinnest ones, which are fully depleted, show higher stability to damp heat treatments than the thicker equivalents [38].

Although the newer thin CIGS cells have shown improvement in V_{oc} and FF, their steep current reduction still remains, and the low current is the primary cause for the thin cells' lower efficiency. The challenge for thinning the absorber with minimal efficiency loss is clearly still open, and this challenge should be mainly directed towards elimination or reduction of the current loss. Analysis of losses in thinner cells should suggest ways for adjusting the deposition methods and improve the thin cells performance.

Analysis of the sub-micron CIGS cells potential is given in Ref. [39]. In this chapter, calculations from this reference are confirmed and expanded.

In Ref. [40] the influence of shunting conductance on device performance is calculated theoretically. With reasonable estimation of parameters, the critical thickness value is 100-300 nm, below which the effect of shunting conductance will likely deteriorate the device performance significantly.

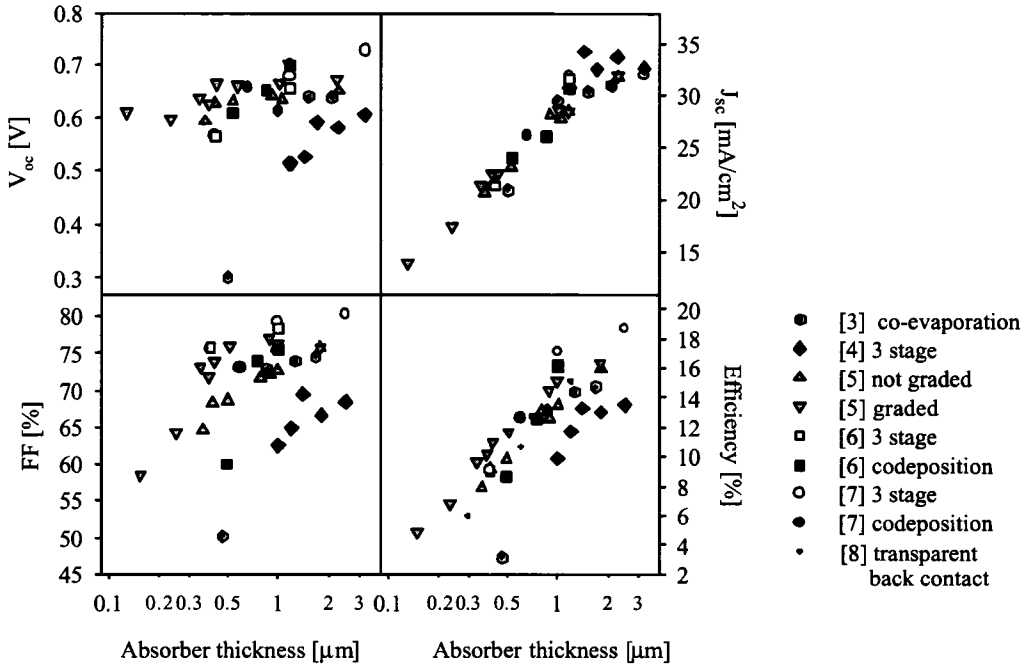

Figure 4.1. Review of experimental reports of CIGS devices with thin absorbers.

4.3. Parameters affected by thickness

4.3.1. Solar cell parameters as a function of thickness

Numerical-simulation results of solar cell performance with reduced thickness (Figure 4.2) qualitatively agree with the experimental data. All of the paraemeters are reduced for thicknesses below 1 μm. The current is reduced by the increasing transparency of the thin CIGS layers and by the recombination at the interface between the absorber and back contact material. If one assumes that the quality of the material remains constant with thickness, the reduction expected is shown with circles in Fig. 4.2. However, it is likely that thinner absorbers have smaller grains, and hence due to

increased recombination at the grain boundaries, the minority-carrier lifetime would decrease with thickness. The dependence of lifetime on absorber thickness in Fig. 4.2 (squares) is assumed to be quadratic, meaning that the grains' linear dimension decreases at the same rate as the absorber thickness, or that the grain boundaries remain columnar [39]. In this case, the open-circuit voltage and the FF, as well as the current, are affected by thinning resulting in a steeper efficiency drop for thinner absorber material.

Note that the current decrease on the experimental data (Fig. 4.1) is much steeper than the simulations predict. This points to the fact that there is an additional loss mechanism not accounted for by these simple arguments. The difference in current decrease with thickness between the simulation and experiment might be due to the grain boundaries treatment. The recombination at the grain boundaries in the model has been accounted for as increased bulk defect density. This approximation holds well if the grain boundaries are not strongly charged [29, 41]. The impact of grain boundaries recombination on the short-circuit current, however, depends on their orientation. Unlike the columnar grain boundaries, that affect the current insignificantly, grain boundaries parallel to the junction can be detrimental for the current [42].

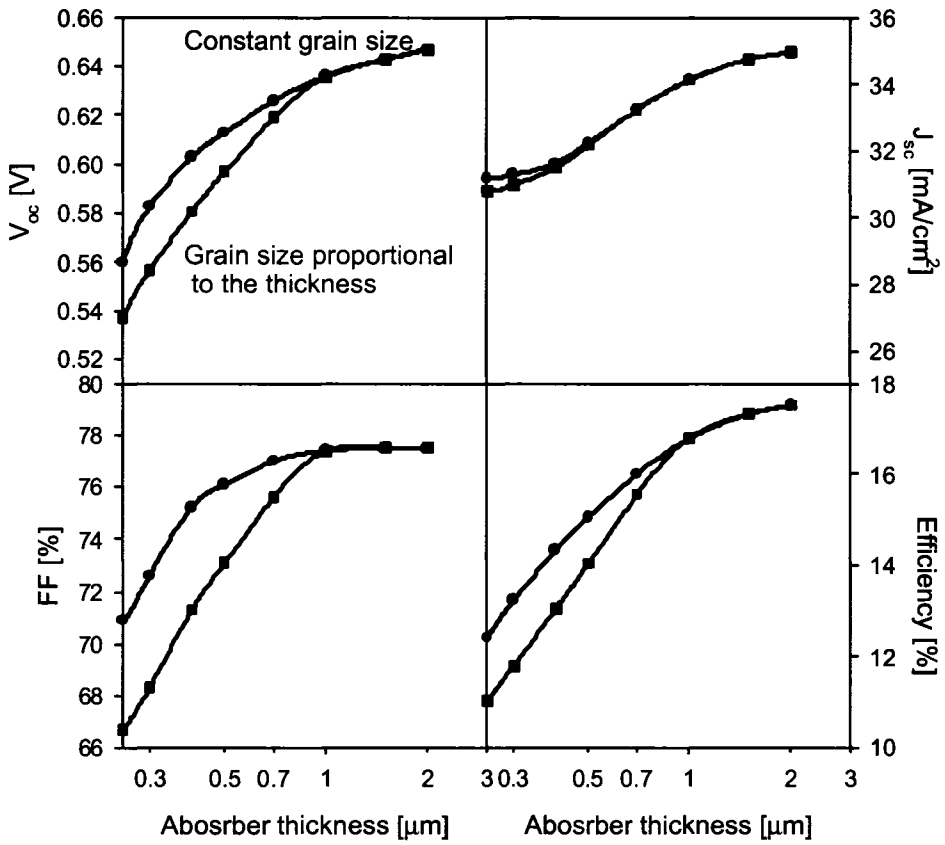

Figure 4.2. Calculated effect of absorber thickness on solar cell parameters with crystalline quality independent of thickness (circles) and with grain size proportional to thickness (squares).

4.3.2. Hole-density variation for different thickness

The calculated impact of the CIGS hole density on devices with different thicknesses is shown in Fig. 4.3. Increased hole density decreases the space-charge region width, resulting in a trade of between voltage and current:

1) The voltage dependence on doping for devices thicker than 1 μm is linear on a semi-logarithmic scale. For submicron devices the voltage follows the same behavior when the thickness of the device is larger than the SCR width. When the device is fully

depleted, however, the voltage benefit of higher doping saturates. The fill-factor of thinner devices varies stronger due to the doping.

2) Current decrease, due to a shorter high-field region with higher hole densities, shows similar trends for different CIGS thicknesses. For thinner devices, however, the current losses at higher carrier densities become more pronounced. For the thinnest device analyzed, d = 250 nm, once the hole density is high enough to lower the depletion region width below the absorber thickness, the current decrease is more abrupt compared to other devices. FF is also affected for very thin absorbers and very high hole densities.

For thick devices ($d \geq 1\,\mu m$), the voltage gain due to increased absorber doping is generally higher than the current loss, and therefore the hole density increase can improve the efficiency. For submicron devices, however, the typical voltage gain is comparable to the current loss, and for ultra-thin devices and high hole densities, the collection losses are high enough to decrease the overall performance. Once the device is fully depleted, the performance is independent of the carrier density (horizontal parts in all parameters at low carrier densities).

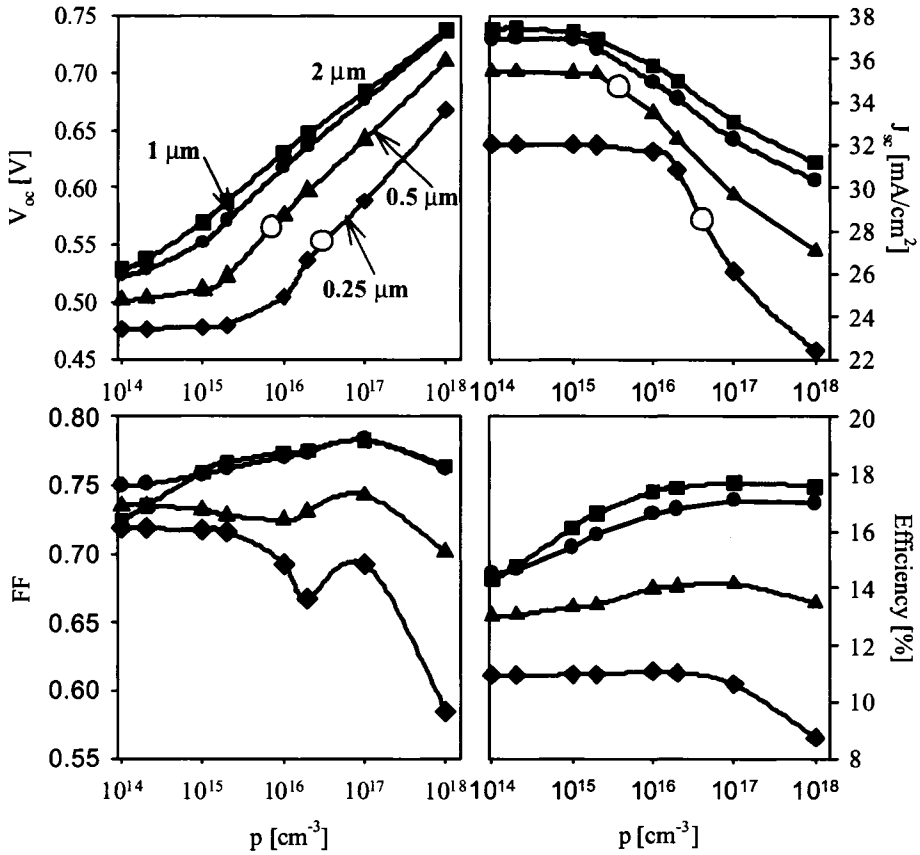

Figure 4.3. Calculated impact of CIGS hole density on V_{oc}, J_{sc}, FF and efficiency for 2 μm (squares), 1 μm (circles), 1/2 μm (triangles) and 1/4 μm (diamonds) device. The points where the device becomes fully depleted are marked with open circles.

4.3.3. Lifetime

The production cost of the CIGS solar cell can be lowered in other ways than reducing the thickness of absorber material. One of them is higher deposition rate, which will lower the deposition time. Other ways are using less pure materials (typically used materials are 99.999 % pure) [35], or lower deposition temperature. The increased rate, decreased purity or lower temperature, however, can increase the defect density in the

absorber material, and thus the minority-carrier lifetime. Additionally, the smaller grain size observed in thinner devices [43] is likely to result in lower lifetimes.

The calculated impact of minority-carrier lifetime on solar cell parameters for devices with different absorber thickness is shown in Fig. 4.4. The lifetimes were varied over wide range, for 4 orders of magnitude. Typical experimental lifetimes for good quality 2-μm CIGS cells are in the 1-2 ns range. Lower lifetimes decrease the voltage as well as the current. The impact of lifetime decrease is higher for thicker devices, due to their larger recombination region. The performance of the thinnest device shown (d = 250 nm), which is fully depleted for the baseline hole density (p = 2 x 10^{16} cm^{-3}), is practically independent of lifetime variations.

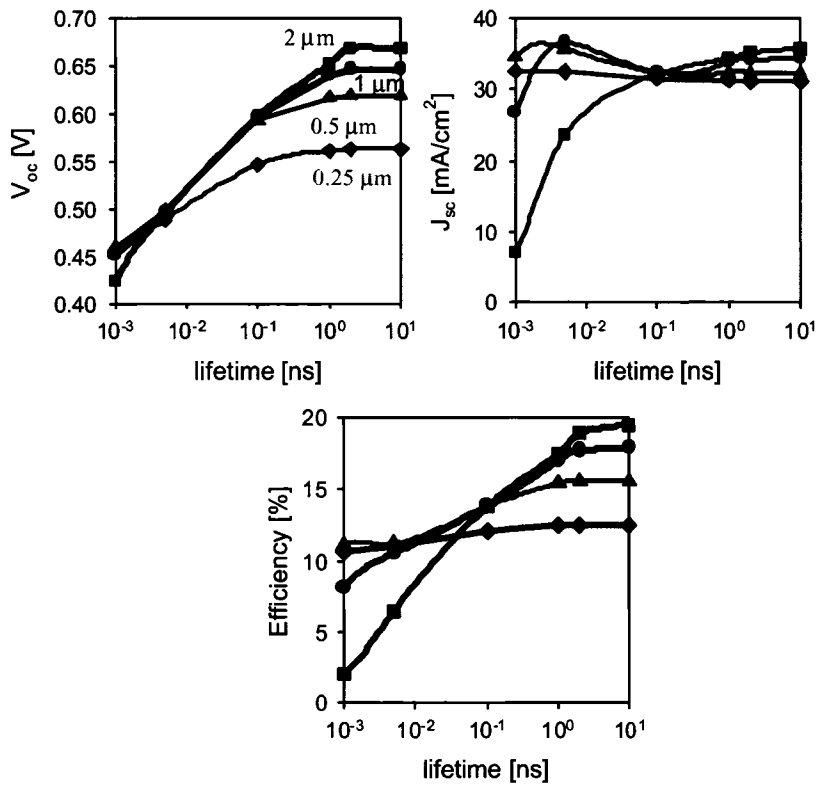

Figure 4.4. Calculated impact of lifetime on solar cell performance for different absorber thickness

4.4. Importance of the back-contact

One of the major differences in thin cells compared to the thicker ones is that the absorber/back contact interface is now located closer to the p-n junction, and the choice of the back-contact material therefore has a high impact on the cell performance.

4.4.1. Back-contact reflectivity

A high optical-reflection coefficient at the back contact can reduce the current losses in thin absorbers. Alternatives to the commonly used Mo that might have superior optical properties are studied in [44]. According to its reflection spectrum, silver is a near-ideal material for the back-contact. However, Ag tends to move thorough the absorber during its growth, and the price of Ag would be a serious obstacle for mass production. Suggested replacements that do not react with the absorber layer and have better optical properties than Mo are W, Nb and Ta.

4.4.2. Recombination at the back contact

As mentioned in Chapter 2, an ideal back contact for thick cells has low resistivity, allows for diffusion of Na from the substrate into the absorber, and blocks the diffusion of other impurities. The optical properties of the back contact material for thick cells are not important, since for thicknesses above 1.5 μm, none of the incident photons can reach the back contact [45]. In thinner cells, however, as the generation profile shifts closer to the back contact, the properties of the back-contact material start to affect the

device performance significantly. Once the thickness of the absorber is lower than $d < W + L_n$, where W is the depletion-region width and L_n is the diffusion length for electrons in the absorber, the recombination for minority electrons at the interface between the CIGS and the back-contact material becomes a significant loss. Current losses due to absorption at the back contact can increase from 1 to 10 mA/cm^2 when the absorber thickness is reduced from 1 μm to 100 nm [44].

4.5. Back-electron reflector

One way to lower back-contact recombination for CIGS absorbers is to add a thin layer that has more Ga than the rest of the absorber. Due to the band-gap difference between $CuInSe_2$ (E_g = 1.02 eV) and $CuGaSe_2$ (E_g = 1.67 eV), the band gap of the material can be altered by varying the In/Ga ratio. The Ga fraction in the absorber affects the band-gap primarily in the conduction band [46]. The band-gap dependence on Ga content in $CuIn_{1-x}Ga_xSe_2$ has been found empirically to be [5]:

$$E_g = 1.010 + 0.626x - 0.167x(1-x) \qquad (4.1)$$

Therefore, with an appropriate spatial variation of Ga in the CIGS, the conduction-band shape can be optimized. The effects of such variation are analyzed below.

A thin Ga-rich layer towards the back of the absorber can reflect the electrons, prevent their recombination at the back contact, and is referred to as electron-back reflector (EBR). The band-diagram of a 500-nm absorber cell with a 10-nm thick EBR is shown in Fig. 4.5. The thin-layer band gap was chosen to be 0.2 eV higher than the rest of the absorber.

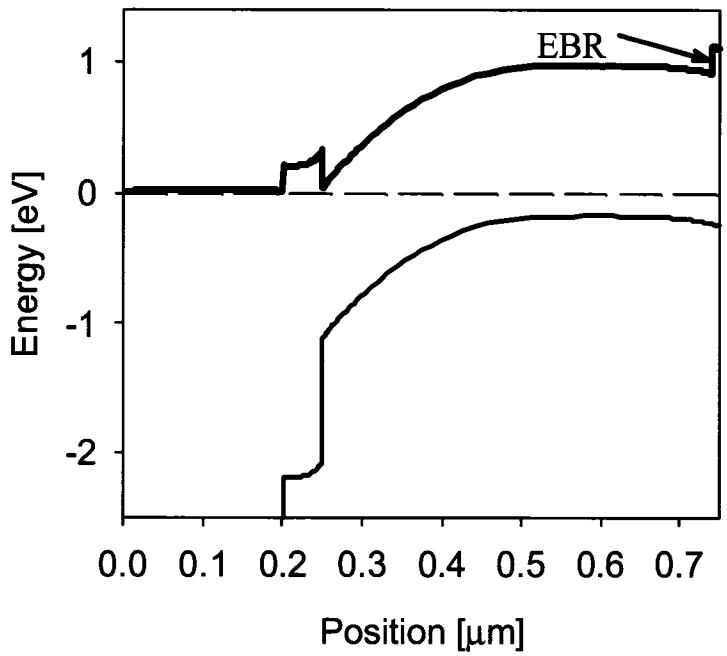

Figure 4.5. A band diagram of a device with added electron-back reflector

The influence of the added electron-back reflector on the solar-cell current is illustrated through the calculated quantum-efficiency curves in Fig. 4.6. The quantum-efficiency curves for devices with a constant 1.15 eV band gap are shown with dashed lines and the ones with added back reflector with solid lines. The light does not penetrate through the 2-μm CIGS layer (Fig. 4.6.a), and thus for this case back reflector addition does not improve the current. Calculations predict a current gain of 1.5 mA/cm^2 for the 1-μm thick CIGS device, and a ΔJ_{sc} = 3 mA/cm^2 for the 500-nm absorber device. The current gain due to the added BR as a function of absorber thickness is shown in Fig. 4.7.

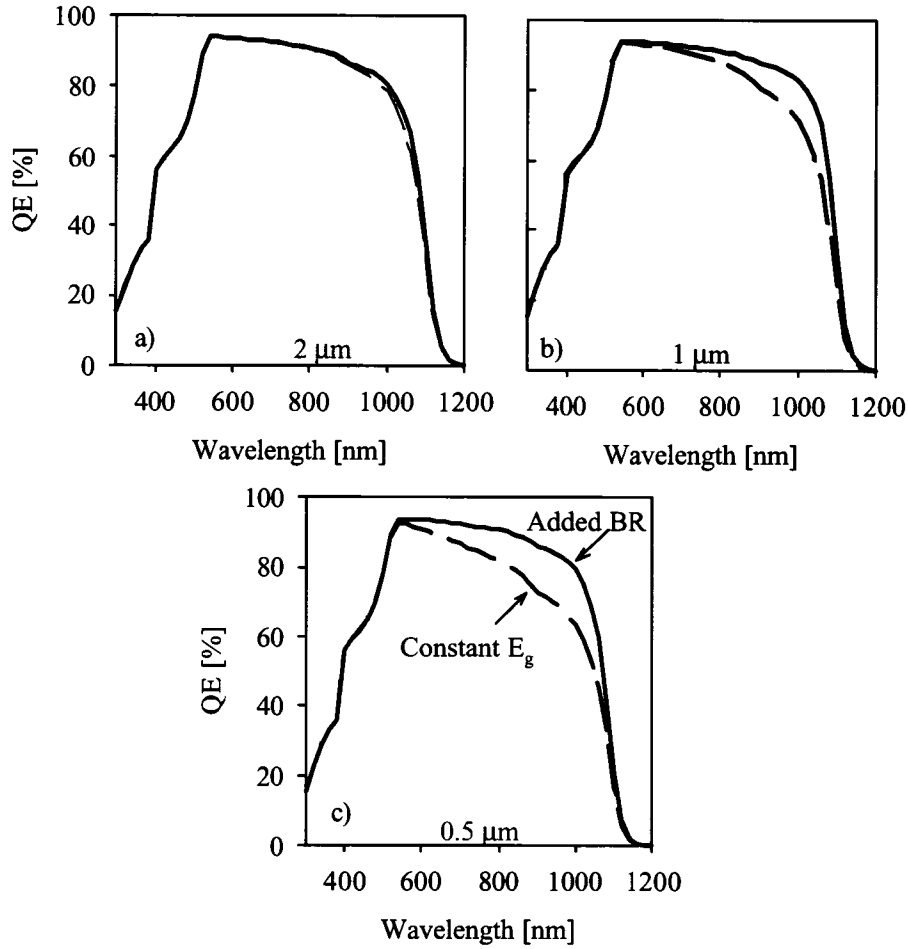

Figure 4.6. The influence of a 10-nm thick, 0.2-eV high back reflector on calculated quantum-efficiency curves for three device thicknesses: a) 2 μm, b) 1 μm, and c) 500 nm

The device performance receives maximum benefit from an EBR when the absorber is slightly thicker (about 100 nm) than the space-charge region width. In that case the CIGS thickness is low enough to allow enough photons to penetrate to the back contact. As the absorbers become thinner, the primary current loss mechanism is incomplete optical absorption, as opposed to back-contact recombination. In fully or almost fully depleted absorbers, the high electric-field region exists throughout the

absorber, it assists the collection of electrons generated near the back contact, and thus the back-reflector benefit is smaller.

The commonly used material for the CIGS back contact, Mo, forms a $MoSe_2$ layer between the back contact and the absorber layer [45, 47]. Formation of the $MoSe_2$ is only possible in presence of Na [48]. The band gap of $MoSe_2$ is 1.2 eV [49]. It is slightly higher than the rest of the absorber, and thus it can act as a modestly effective electron reflector.

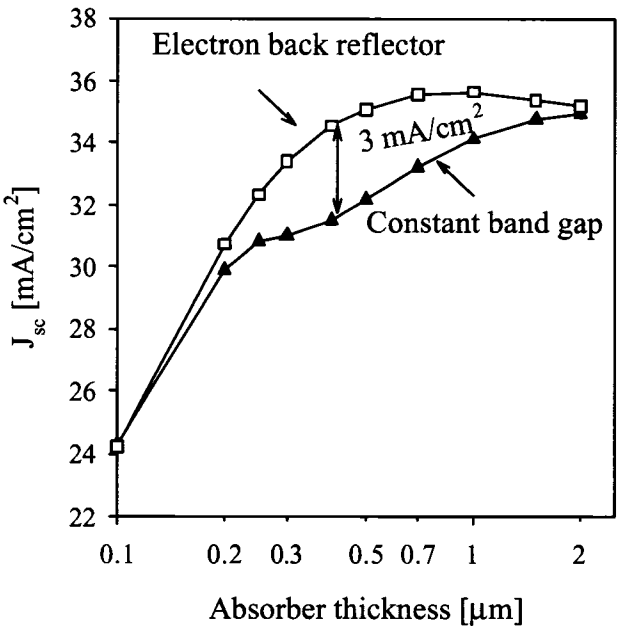

Figure 4.7. Short-circuit current as a function of absorber thickness in cells with constant band gap (filled symbols) or with an electron back reflector (open symbols)

4.5.1. Electron-back-reflector height

In the previous results, the EBR height was taken to be 0.2 eV. The effect of electron-back reflector of different heights for a 1-μm absorber and a 500-nm-thick

absorber is shown in Fig. 4.8. For the 500-nm device the current increase is larger and there is a FF improvement, both resulting in a higher percentage efficiency gain for the thinner device. An electron back reflector of 0.1 eV or less has little impact on the performance. The benefits of the EBR height increase steeply between 0.1 eV and 0.2 eV, and there are little additional improvements for reflectors greater than 0.2 eV. In order to simulate the grain boundary recombination, the 500-nm thick device has 4 times higher defect density ($\tau \sim d^2$) than the 1-μm thick one. This lowered lifetime results in lower voltage and fill-factor for the thinner device. If the grain boundary recombination is not accounted for, the difference between the V_{oc} and FF values for the thinner and the thicker cell will be smaller, but the trends for EBR addition will be equivalent.

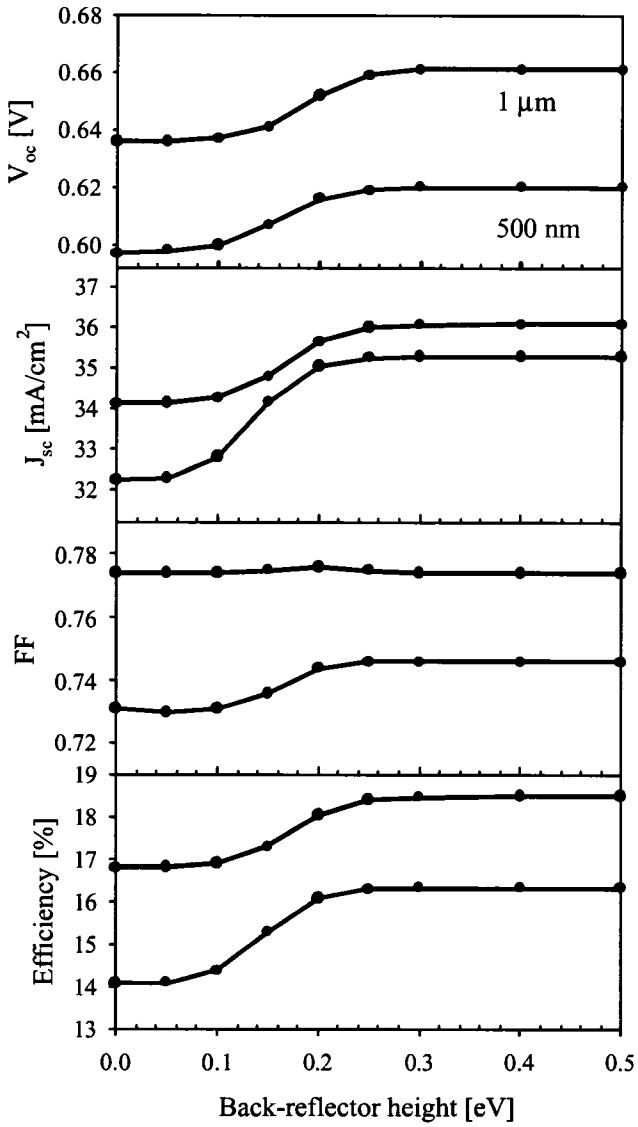

Figure 4.8. Impact of electron back-reflector height on all solar cell parameters

4.6. Band-gap grading

Diffusion between the Ga rich and Ga poorer layers will cause intermixing between them. Thus, an abrupt electron back reflector as shown in Fig. 4.5 is mathematical idealization, and physically the absorber will have a graded band gap. The

effect of band grading on solar-cell performance and the optimal grading profile has been extensively studied ([50, 51] and the references therein).

The effect of band-gap grading with variations in absorber thickness is analyzed below. The band gap is assumed to be a linear function of position. A schematic of a double graded absorber is shown in Fig. 4.9. The back-side grading (in CIGS towards the back contact) is marked with x_{gBa} and the front side grading (towards the junction) with x_{gf}. The optimization of grading profile is divided into 2 parts: only back grading and double grading. Usually the 3-stage process produces double graded absorbers. The Ga/(In+Ga) ratio can be varied during the deposition process, by varying the fluxes of different elements. The record efficiency cell has $x_{gBa}/d \sim 0.80$ and $x_{gf}/d \sim 0.2$ [52].

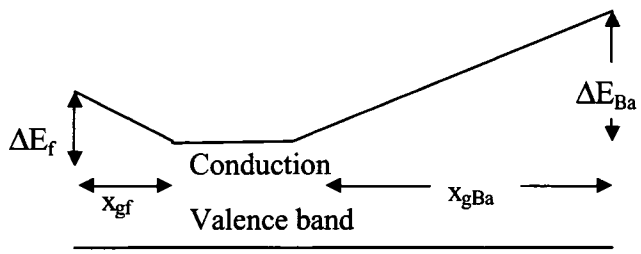

Figure 4.9. Band gap profile.

4.6.1. Parameterized back-grading profile

As with an abrupt back reflector, back grading lowers the back-contact recombination and provides an additional electric filed that improves minority carrier collection. In order to find the optimal back grading, the point where grading starts, x_{gBa}, the height of the grading, ΔE_{Ba}, or both, can be varied.

Calculation results for the x_{gBa} variation, while keeping ΔE_{Ba} fixed, are shown in Fig. 4.10. Grading has a greater benefit for devices thicker than 500 nm, then for the ultra thin ones. The optimal start of the grading depends on absorber thickness. For thickness of 1 μm, the optimal situation is for x_{gBa} ~ 60 % of the absorber thickness, while for thinner devices it is better if the grading is confined closer to the back contact. For thinner devices, 500-nm and 250 nm thick CIGS, the grading it is less beneficial.

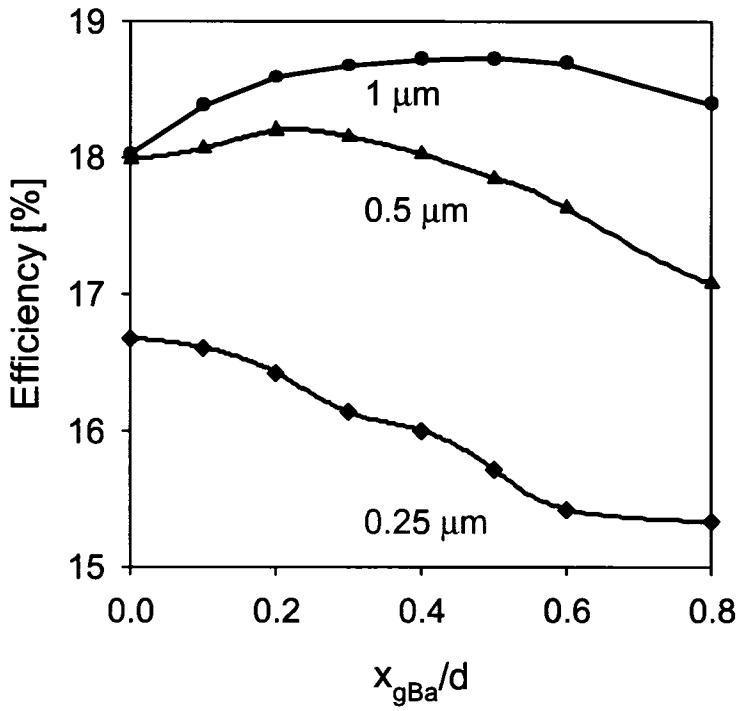

Figure 4.10. Influence of the back grading starting point on the cell efficiency for ΔE_{Ba} of 0.2 eV.

4.6.2. Back-grading slope

Increasing the grading slope can increase the electric field and thus virtually increase the minority carrier diffusion length. For a case of fixed x_{gBa} at 60% of the

absorber thickness, the impact of variation of ΔE_{Ba} on the device efficiency is shown in Fig. 4.11. For a lower quality absorber material, the electric field created by larger conduction-band slope becomes more beneficial since the lower quality materials experience collection problems. At the same time, Ga addition increases the defect density. This is especially harmful for thin absorbers, when the high Ga-high defect layer comes close to or inside the space-charge region. The two effects balance each other and the efficiency improves until 0.2 eV and saturates afterwards. $x_{gBa} = 0$ assumes a back reflector. That way the effect of grading can be separated from the back-contact passivation.

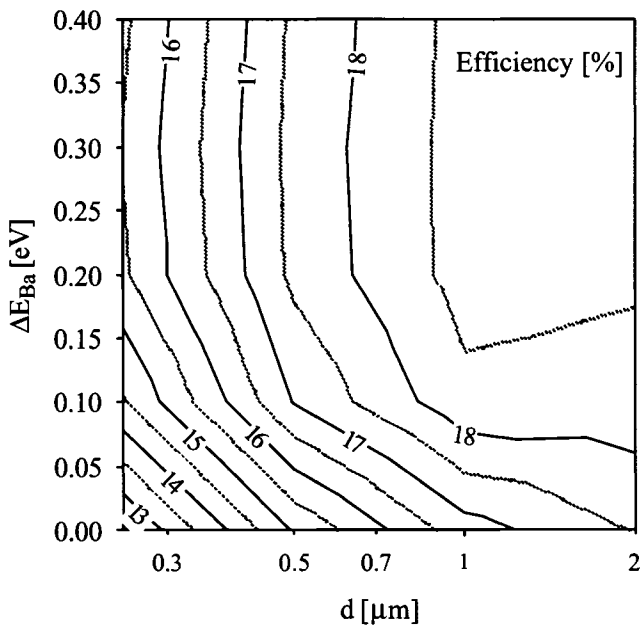

Figure 4.11. Influence of the back grading slope on the cell efficiency

4.6.3. Double grading

Front grading as an addition to back grading can be somewhat beneficial and increase the device voltage. The beneficial effects happen if the slope is low enough and the graded region is confined within the space-charge region. Otherwise, the front grading creates reverse fields that lower the collection. Then, the small voltage increase due to front grading is neutralized by FF losses.

4.7. Sensitivity to parameter fluctuations

The discussion above has assumed that although solar cell parameters may change as the CIS absorber is thinned, they are spatially uniform over the cell. Some of the parameters sensitivity has been explored. Section 4.3.3, for example, shows that a difference in lifetime has more effect on thicker devices than the thinner ones. In the following chapter, we will explore the additional problem of how spatial nonuniformities can affect the CIGS cell performance.

CHAPTER 5

NONUNIFORMITIES IN THIN CIGS SOLAR CELLS

5.1. Introduction and literature review

CIGS is a polycrystalline material, and thus, inherently nonuniform. In this type of materials grains vary in size and structure, leading to variations of several electronic parameters throughout the device. Variation in parameters can also be observed within a single grain, between the boundaries and the bulk.

Despite many attempts to analyze the effect of polycristallinity on the thin cell performance, the impact of nonuniformities in a number of materials is not well understood. For example, the effect of potential fluctuations is known to affect the transport of other materials such as polycrystalline Si [53].

Nonuniformities have been directly observed in both CIGS and CdTe devices by several different techniques: OBIC, EBIC, LBIC and scanning-tunneling microscopy (STM). A review is given in Ref. [54].

Extensive theoretical studies of nonuniformities in polycrystalline devices, mainly in CdTe, are given in Ref. [54-58]. The nonuniform device in Ref. [54-58] is approached at as a linear array of microdiodes, whose voltages satisfy an assumed probability distribution function. The variable-voltage region is substituted by a single foreign diode in a homogenous medium. If the foreign diode has a voltage larger than the rest of the device, then strong forward currents localize the perturbation over a small distance. If the foreign diode has lower voltage, however, then it is in forward bias provided by the surrounding diodes. This causes lateral currents through the TCO, and the voltage drop is $\Delta V = \rho J_o L^2$, where ρ is the sheet resistance in the TCO, $I = J_o L^2$ is current, and L is the length over which the influence of the weak diode is felt, referred to as screening length. Unlike a low-voltage diode that affects only the forward-bias part of the current-voltage characteristics, a leakage path affects the reverse bias as well.

Band–gap fluctuations have been theoretically shown to have detrimental effect on CIGS solar cell performance [59-62]. Local series resistance from an intrinsic ZnO (i-ZnO) layer was found to decrease the performance loss caused by the nonuniform band gap. Local resistance can be approximated as a series resistance connected to an individual diode. It is different than the "distributed" resistance which can support voltage drop in direction parallel to the junction. For a particular model, there is an optimal value of the local resistance that minimizes the damage done by the nonuniformities.

This chapter will analyze the losses that can be expected by nonuniformities on thin CIGS cells. It is organized in four parts:

The first part investigates the impact that variations in different parameters have on the device performance, especially on the open-circuit voltage, and whether devices with submicron absorbers are more sensitive to these variations.

The second part analyzes the impact that area with different open-circuit voltage has on the rest of the device, which generalizes the impact of all the electronic parameters on the device performance. The open-circuit voltage can be analytically calculated when the parasitic resistances are neglected. The 2-dimensional approach allows for analysis of the weak area distributions.

The third part introduces the parasitic resistance as a distributed resistance. It explains the relationship between the distributed resistance and a series resistance of a single diode, and it then calculates the effect of distributed resistance on the cell parameters.

The fourth part determines the impact that nonuniformities perpendicular to the junction have on the CIGS cell efficiency.

5.2. Parameter sensitivity

Some attempts to produce CIGS absorbers with reduced thickness have resulted in less uniform devices. In addition to being less uniform, thinner CIGS cells might also be less forgiving to nonuniformities in different electronic parameters. The focus here will be on nonuniformities in open-circuit voltage, because they affect the device

performance much more severely than nonuniformities in the current. The influence of different parameters on the device open-circuit voltage is investigated below.

5.2.1. Band-gap fluctuations

Figure 5.1. shows open-circuit voltage dependence on 200-meV band-gap variations from the baseline value of 1.15 eV for four different CIGS thicknesses. The E_g dependence on voltage is linear, and the slopes are independent on thickness. The variations in band gap will affect the V_{oc} of thin and thick devices equally.

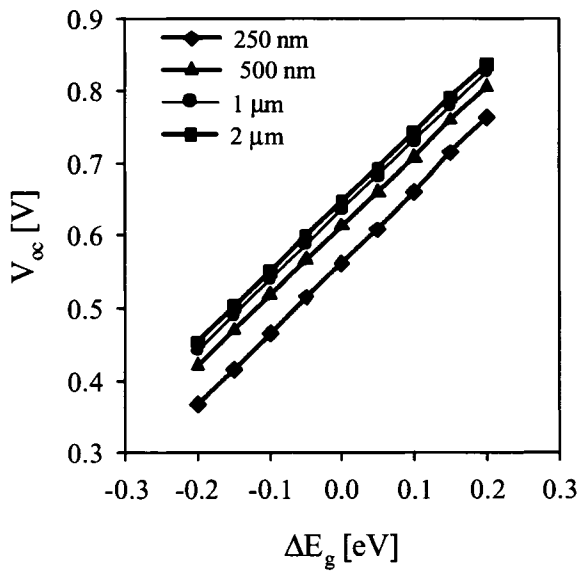

Figure 5.1. Impact of band-gap variation on the open-circuit voltage

5.2.2. Thickness nonuniformities

Nishiwaki et al. [63] has reported AFM (atomic force microscopy) data from devices with different thickness. The surface roughness of the absorber was 0.3-0.4 μm

regardless of its thickness. That means that the thinnest device produced, with a 0.47-μm thick absorber, had areas with major thickness variations. It is likely that in some areas the Mo back contact was not completely covered by CIGS and the device was partially shunted.

The calculated V_{oc} dependence on thickness variation is shown in Fig. 5.2. Voltage of the thinner devices is significantly more sensitive to variation in thickness. Thickness variations in Fig. 5.2 are presented as a percentage of the initial thickness. 50% thickness variation, (equal to 125 nm for the thinnest device analyzed, or to 1 μm for the thickest), will lower V_{oc} of the 250-nm devices by 100 mV, and the voltage of the 2-μm devices about 10 mV.

The difference on an absolute thickness scale is more dramatic. 125 nm thickness variations would affect the 250-nm thick device the same as shown in Figure 5.2, but the impact of the same variation on the thicker device voltages would be negligible.

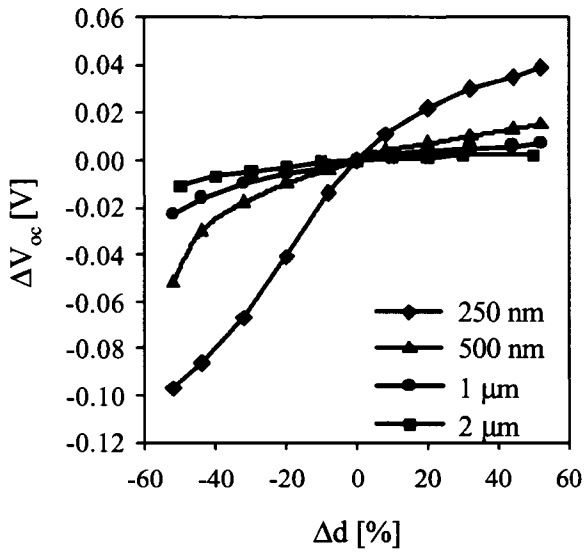

Figure 5.2. Impact of device thickness variations on the open-circuit voltage.

5.2.3. Lifetime variations

Thinner devices are likely to have smaller grains, and the recombination at their grain boundaries is likely to lower the minority-carrier lifetimes. Voltage change that can be expected for lifetime variation over four orders of magnitude is shown in Fig. 5.3. Submicron devices have smaller recombination volume, and are therefore less sensitive to lifetime variations, though as seen in Fig. 5.1, they start from a smaller V_{oc}.

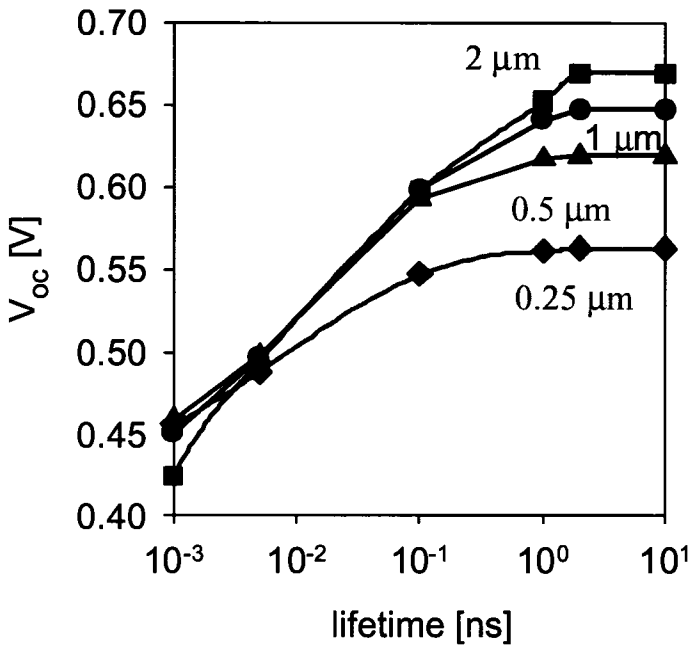

Figure 5.3. Calculated decrease in voltage dependence on the minority carrier lifetime

5.2.4. Parameter sensitivity with thickness

A summary of the calculated J-V parameter sensitivity as a function of thickness is shown in Fig. 5.4. The baseline cell corresponds to the highest efficiency 1-μm thick

cell fabricated to date [64]. All of the solar-cell parameters experience reduction at thickness lower than 1 μm, which becomes much steeper below 500 nm. This confirms that roughness will affect the thinnest devices more severely. As shown before for V_{oc}, high lifetime is more important for standard thickness devices. The dependence is similar for any of the J-V parameters. Reduced hole density (filled circles) decreases the voltage, but increases the current, since wider depletion means better collection. The overall effect on the conversion efficiency is negative, and its thickness dependence does not vary significantly for different hole densities.

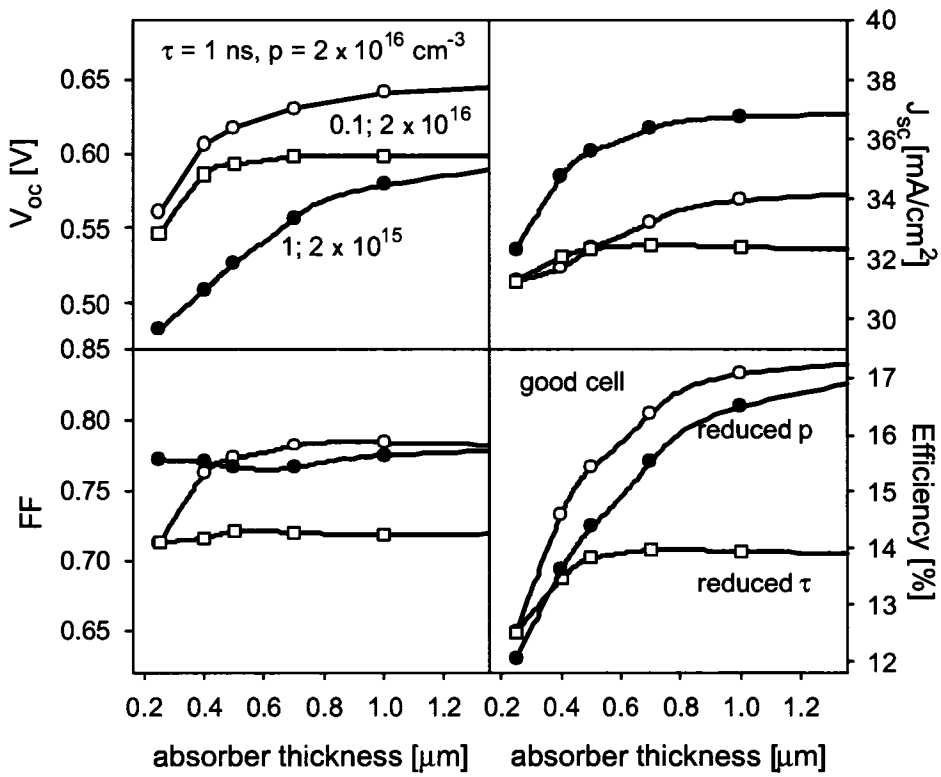

Figure 5.4. Parameter variation as a function of thickness. Lower lifetime and decreased carrier density dependence also shown.

5.3. Nonuniformities parallel to the junction (lateral)

Once the influence of the electronic parameters on voltage is known, the effect of an area with different voltage on the device performance can be determined. A nonuniform device in this model consists of weak and stronger diodes.

In order to calculate the impact of weaker area on the overall device performance, the standard equivalent-circuit model (Fig. 3.3.) needs to be replaced with a network of diodes connected in parallel. A schematic of the two-dimensional circuit is shown in Fig. 5.5. The actual model has 10 x 10 array of diodes, but only 5 x 4 are shown here. The diode with properties different than the rest of the device, referred to as "weak diode" is located in the middle unless stated otherwise and is highlighted in Fig 5.5. An alternative current path, or partial shunt, is also shown.

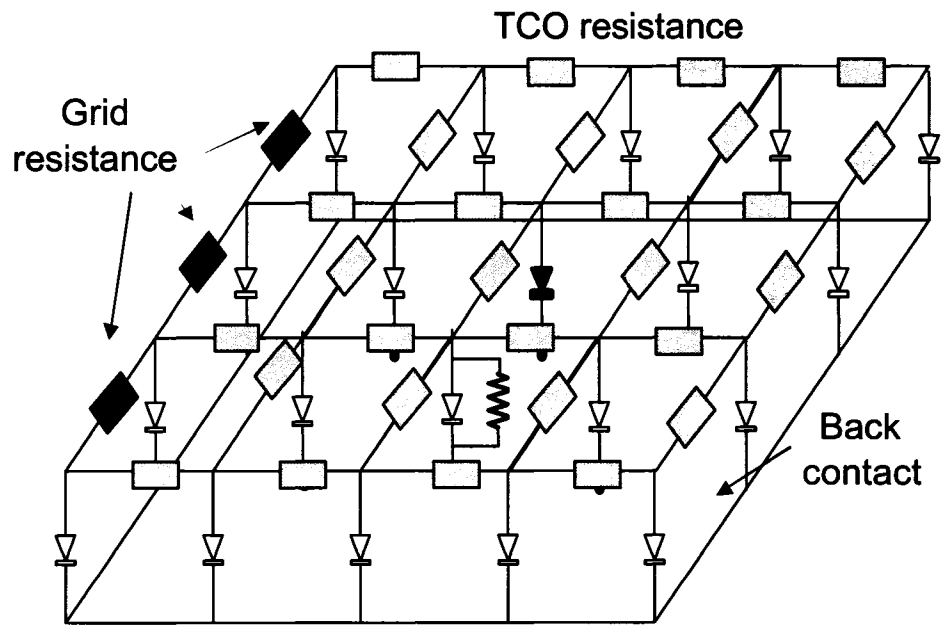

Figure 5.5. A schematic of an equivalent circuit representing a nonuniform device.

5.3.1. V_{oc} of nonuniform device without R_s

In first approximation, the diodes are not separated by resistance. The total current of the cell is sum of all the diode currents, independent of the diodes spatial distribution. A device with area $A = nA_1$, can be represented by n diodes connected in parallel, each with area A_1. Then, the I-V relation is:

$$I = \sum_{i=1}^{n}\left[I_{oi}\left(\exp\left(\frac{qV}{AkT}\right) - 1 \right) - I_{Li} \right] \quad , \tag{5.1}$$

where n is the total number of diodes, A is diode quality factor, I_{oi} is diode saturation current and I_{Li} is light-generated current for the i-th diode.

It is assumed that the light-generated current is uniform throughout the device, and that there are only two types of diodes: "strong" diodes with higher open-circuit voltage (V_{ocs}), and "weak" diodes with lower open-circuit voltage (V_{ocw}). The number of the "strong" diodes is taken to be s, the number of "weak" diodes w, and s + w = n. The open-circuit voltage of the nonuniform devices is calculated to be:

$$V_{oc} = V_{ocs} - \frac{AkT}{q}\ln\left[1 - a + a\exp\left(\frac{q\Delta V_{oc}}{AkT}\right)\right] \quad . \tag{5.2}$$

Here $\Delta V_{oc} = V_{ocs} - V_{ocw}$ is the difference between the open-circuit voltages of the strong and weak diode, and $a = \frac{w}{n} = \frac{A_w}{nA_1} = \frac{A_w}{A_{tot}}$. is the ratio of the weak area A_w to total area A_{tot} of the device. For large areas and large differences in voltage, the voltage dependence on the weak area is logarithmic, and it is linear with ΔV_{oc}. The diode quality factor is assumed to be the same for strong and weak areas and hence the fill-factor FF

depends only on the open-circuit voltage [14]. These relationships are calculated and plotted in Fig. 5.6.

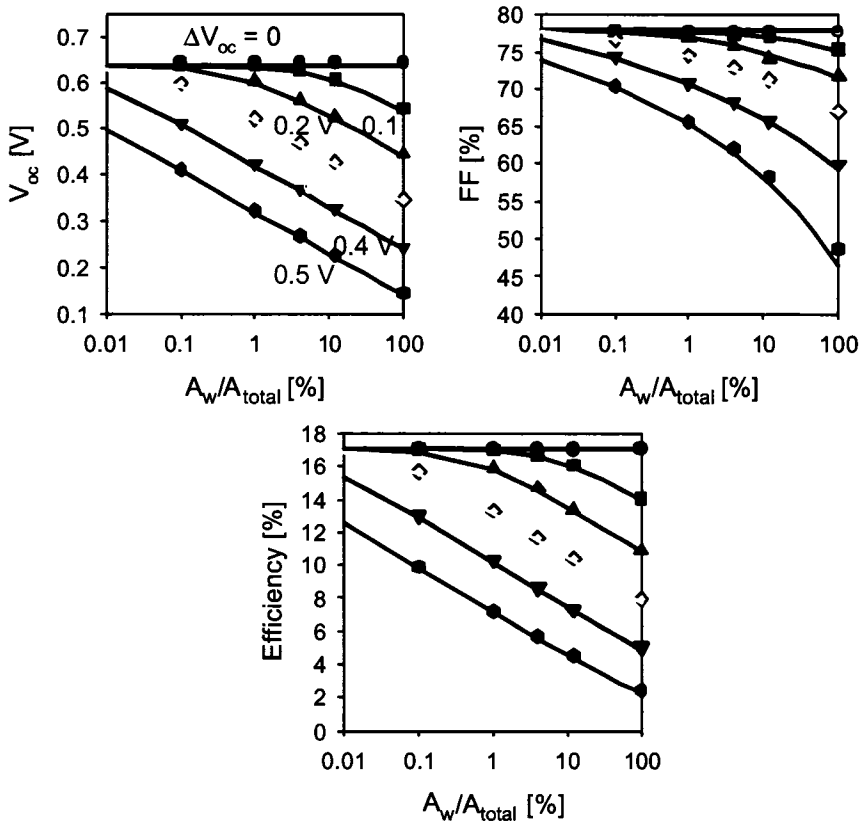

Figure 5.6. V_{oc}, FF, and efficiency dependence as a function of the weak area calculated analytically (lines) and numerically (symbols)

5.3.2. Linear vs. distributed resistance

When series resistance is not negligible, equation (5.1) can not be solved analytically without additional assumptions, and numerical methods are therefore necessary. One way to analyze the impact of nonuniformities is a diode network model such as in Fig. 5.5.

The grid resistance is assumed to be significantly lower than the TCO resistance. The value used is $R_g = 30$ mΩ. The back-contact layer resistance is assumed to be negligible. Usually, the TCO resistance is much smaller than the resistance of the semiconductor layers, and therefore any lateral current flows through this layer.

The TCO resistance is proportional to the series resistance of a single diode. The conversion can be derived by determining the power loss due to the current flow in the TCO layer. The relation as derived in [65, 66] is:

$$Rw^2 = 3R_s \qquad (5.3)$$

here R_s is the series resistance of one diode – linear series resistance, R is the sheet resistance of TCO, also referred to as distributed series resistance, and w^2 is the device area. The units for R_s are Ω-cm^2, and for R are Ω, but very often it is presented in Ω/square. Fig. 5.7 shows J-V curves of 1 diode and 10 x 10 -diode system, where the resistances are calculated according to equation (5.3). For low series resistance, there is good agreement between the curves. For high sheet resistances or large-area devices, there is significant difference between the linear and distributed-resistance curves. The disagreement between the curves increases with applied voltage bias. This means that the approximation used will not introduce too large error when the conversion efficiency is determined, but much higher error when calculating the diode quality factor and the device series resistance. A reasonably well performing solar cell should have series resistance lower then 3 Ω-cm^2, and thus the distributed resistance approximation can be well used.

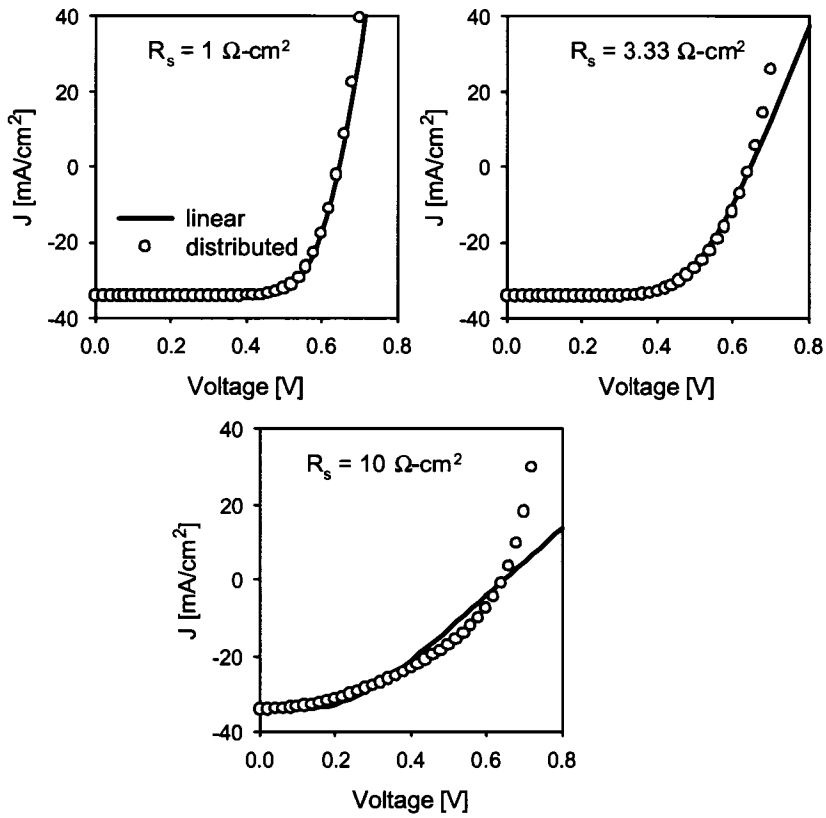

Figure 5.7. J-V curves of a single diode with linear series resistance R_s (lines) and a 10 x 10 diode circuit with a distributed resistance (symbols).

5.3.3. Impact of TCO resistance

Fig. 5.8 illustrates the impact of the weak area on the rest of the device for two TCO resistances. It shows a voltage-difference map $\Delta V(x, y)$ between the voltage map for a uniform strong device and the voltage map when 4% of the device area is weakened. The weak area in this case is located in the middle of the device. The open-circuit voltage of an isolated strong diode is V_{ocs} = 0.65 V and of an isolated weak diode is 0.25 V. The applied voltage is 0.5 V.

In case of higher TCO resistance, Fig. 5.8.a), the voltage dip in the center of the solar cell is deeper than that for the lower resistance situation (b). The larger TCO resistance results in a higher voltage drop in TCO, and partially isolates the weak diodes from the rest of the device. This agrees with the concept of screening length [54, 55, 57, 58], marked on Fig. 5.8.a). The screening length for the lower TCO resistance case extends to the end of the device.

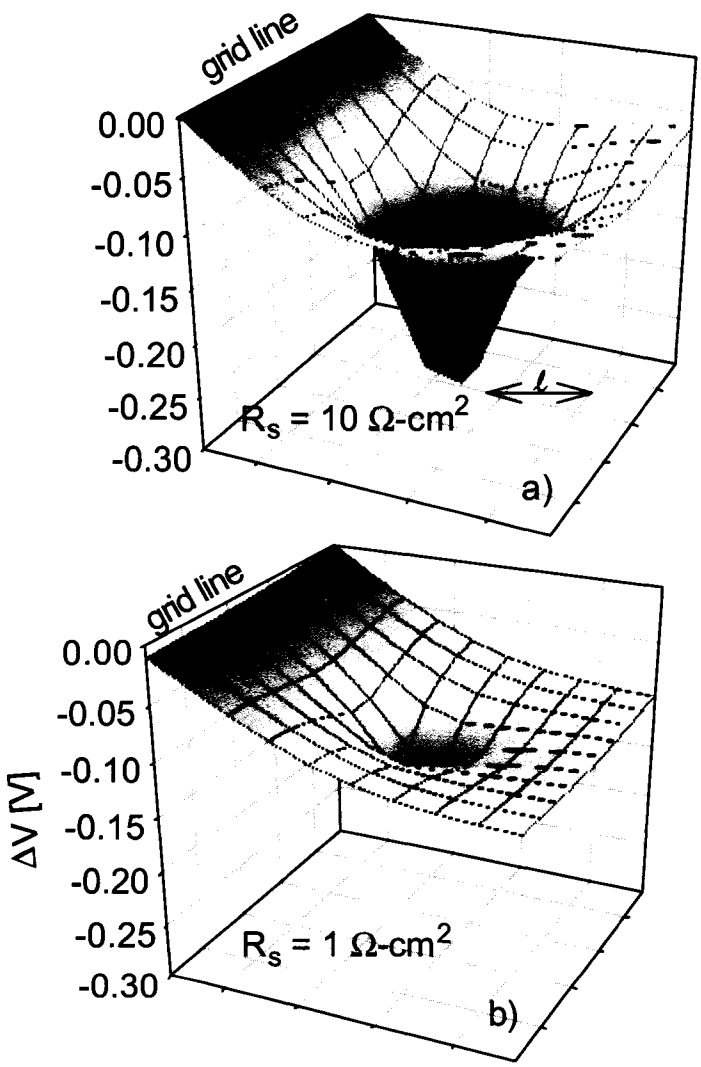

Figure 5.8. The impact of TCO resistance on the voltage map for a) R_s = 10 Ω-cm^2 and b) 1 Ω-cm^2.

Figure 5.9. shows numerically obtained results for the TCO-resistance influence on the solar-cell performance. The V_{oc} of the weak diodes is 0.4 V lower than of the rest of the device.

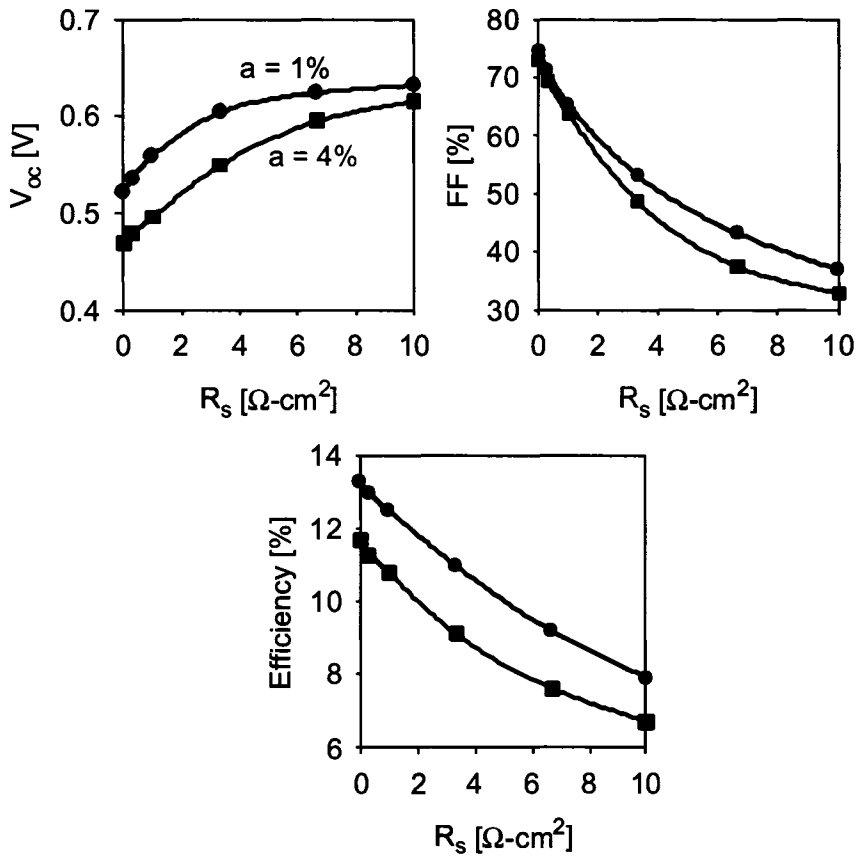

Figure 5.9. The impact of TCO resistance on the nonuniform device performance

The TCO resistance can mitigate the voltage loss by more than 100 mV for this particular model. However, the TCO resistance also reduces the FF of the entire device. The percentage FF loss will always be more than the voltage gain, and thus the effect on the efficiency is always negative.

Since the weak diodes "pull down" their strong neighbors, the distribution of the weak diodes in the device should have an effect on voltage (Fig. 5.10). A weak area that takes 4% of the total area is least detrimental to the total device voltage if all of the weak diodes are clustered together and located towards one of the corners. That way the weak diodes have the fewest nearest neighbors to influence. For the same reason, the voltage of clustered weak diodes in the middle of the device is higher than the voltage of a device with the same area taken by weak diodes, but scattered throughout the device. Although different distributions impact the V_{oc} of the solar cell to different degrees, the maximum-power point, and thus the conversion efficiency remains essentially unchanged.

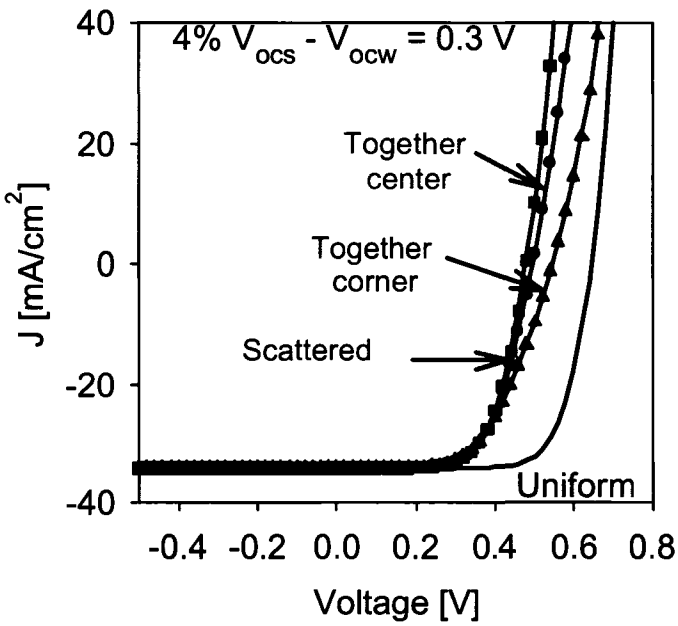

Figure 5.10. Effect of weak-area distribution on J-V curves

5.3.4. Analytical approach

To implement the effect of the TCO into the diode equation, and to confirm the numerical results, more severe approximations then the ones in 5.3.1 need to be made. If it is assumed that the voltage map is independent of the voltage bias, and voltage maps in Fig. 5.8 can be approximated as:

$$V(r)=\begin{cases} V_w & r \le a \\ V_w + \dfrac{\Delta V}{l} r & a \le r \le (a+l) \\ V_s & (a+l) \le r \le L \end{cases} \qquad (5.4)$$

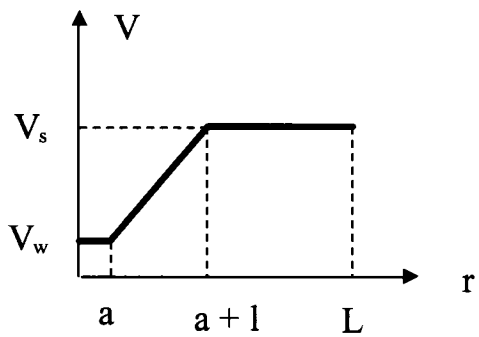

Figure 5.11. A linear approximation of a voltage map in polar coordinates

The current in the nonuniform device is then an integral of the currents in individual diodes:

$$I = \int 2\pi r\, dr \left\{ J_0 \left[\exp\left(\frac{qV(r)}{AkT} \right) - 1 \right] - J_L \right\}, \qquad (5.5)$$

i.e. the effect of nonnegligible TCO resistance is implemented in the diode equation as a voltage dependence on position. The device behavior can be divided in 3 parts: weak-diode area (r < a), screening-length area (a < r < a + l) and strong area unaffected by the

weak diodes (a + l < r < L). The results are shown in Fig. 5.12. The results made with this approach follow the trends obtained by the numerical methods. However, analytical results due to many assumptions show differences especially in the weak vs. strong area ratio.

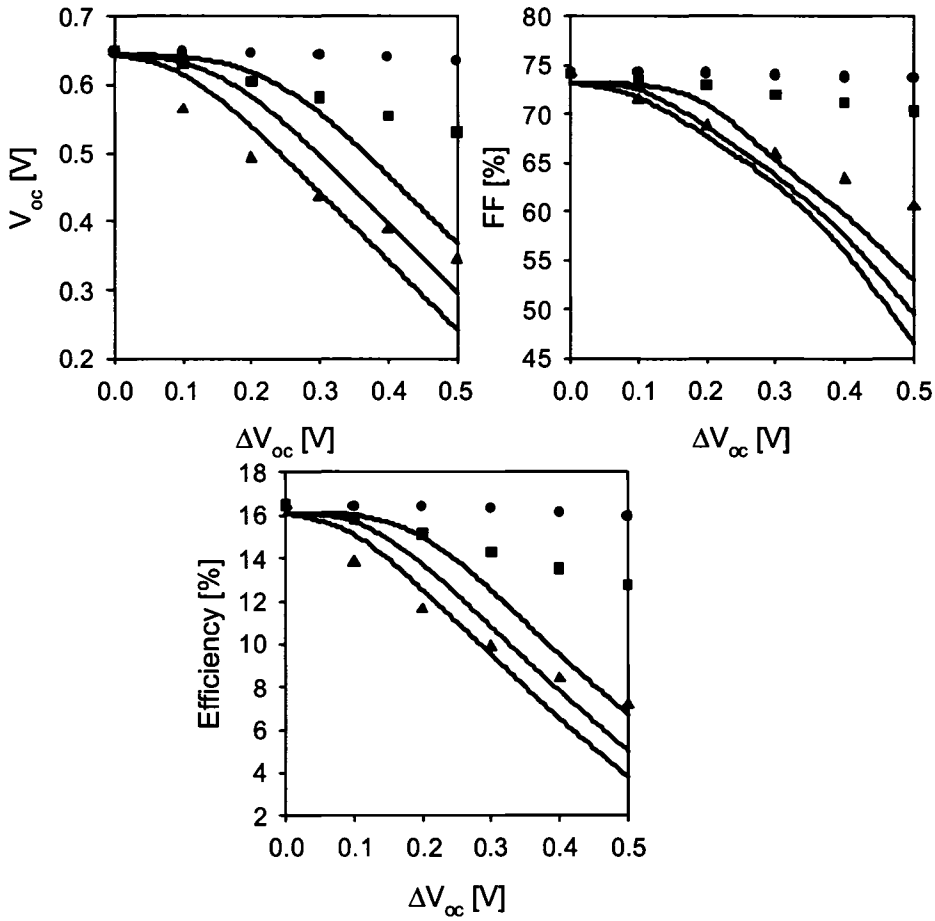

Figure 5.12. Analytical solutions (symbols) compared to numerical (lines) for the solar cell parameters dependence on the weak area properties. The weak area is 1% of the total area (black-circles), 4% (red-squares) and 12% (blue-triangles)

5.3.5. Difference between a low-voltage diode and a shunt

Although an extremely weak, low-voltage diode can lead to shunting, the mechanisms behind them are different, and the effect on J-V curve is different as well. Fig. 5.13 shows PSpice simulation results when the middle diode in the 10 x 10 circuit has a lower voltage (Fig.5.13. a) and when there is a shunt resistor connected in parallel, which allows an alternative path for current flow (Fig. 5.13. b). As opposed to a low voltage diode, which lowers the voltage and the fill factor and does not affect the reverse bias behavior, a shunt is visible in both forward and reversed bias, and primarily affects the FF, although in extreme cases, it can also lower the voltage.

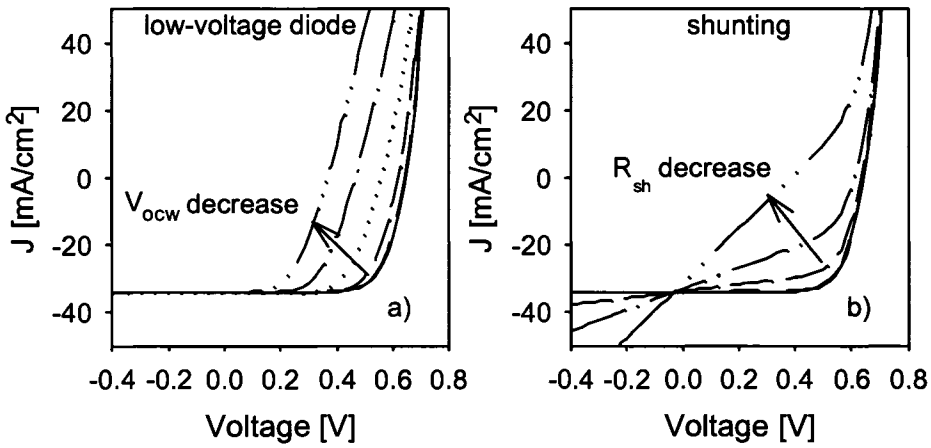

Figure 5.13. An impact on J-V curves of a) low-voltage diode and b) finite shunt resistance

5.4. Nonuniformities perpendicular to the junction

In addition to nonuniformities in the lateral direction, the influence of nonuniformities in direction perpendicular to the p-n junction can also affect the device performance, especially in a solar cell with noncolumnar grains.

Perpendicular nonuniformities have been studied by introducing an oscillatory parameter behavior. This has been simulated with a scale-like function shown in Fig. 5.14. The results are sensitive to whether the higher value of the parameter is closer or further away from the p-n junction. For band-gap variations, for example, improved performance is obtained when the band-gap has higher values close to the junction. There is not an obvious physical reason, however, to assume a higher probability for one situation than the other. To determine the overall impact of variable parameters, the cell performance in both scenarios has been calculated and then averaged. Note that there is always an entire period of variations within the space-charge region (The SCR width in this model is 270 nm). Figure 5.14 shows band-gap variations, but the same model has been applied for lifetime and doping fluctuation analysis.

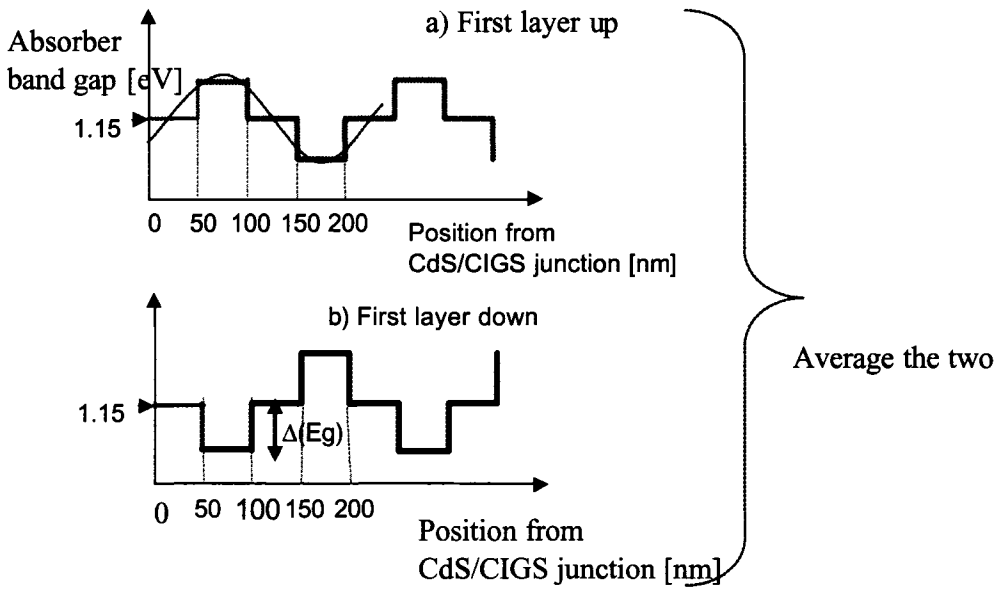

Figure 5.14. A scale-like function simulating oscillatory behavior of the electronic parameters

Calculation results for a variable band-gap in the direction perpendicular to the junction for different thicknesses are shown in Fig. 5.15. Although slight variations (~ 50 meV) can result in a small voltage increase, for higher fluctuations amplitude, the voltage always drops. The drop is more pronounced for thicker devices. It is interesting to note that voltage drops due to band-gap fluctuations $\Delta E_g > 0.15$ eV become independent of thickness. The reversed electric fields confine the light-generated carriers within a small distance from the p-n junction, and thus the bulk of the absorber plays a little role in the device voltage. The same reversed fields are the cause for the FF loss.

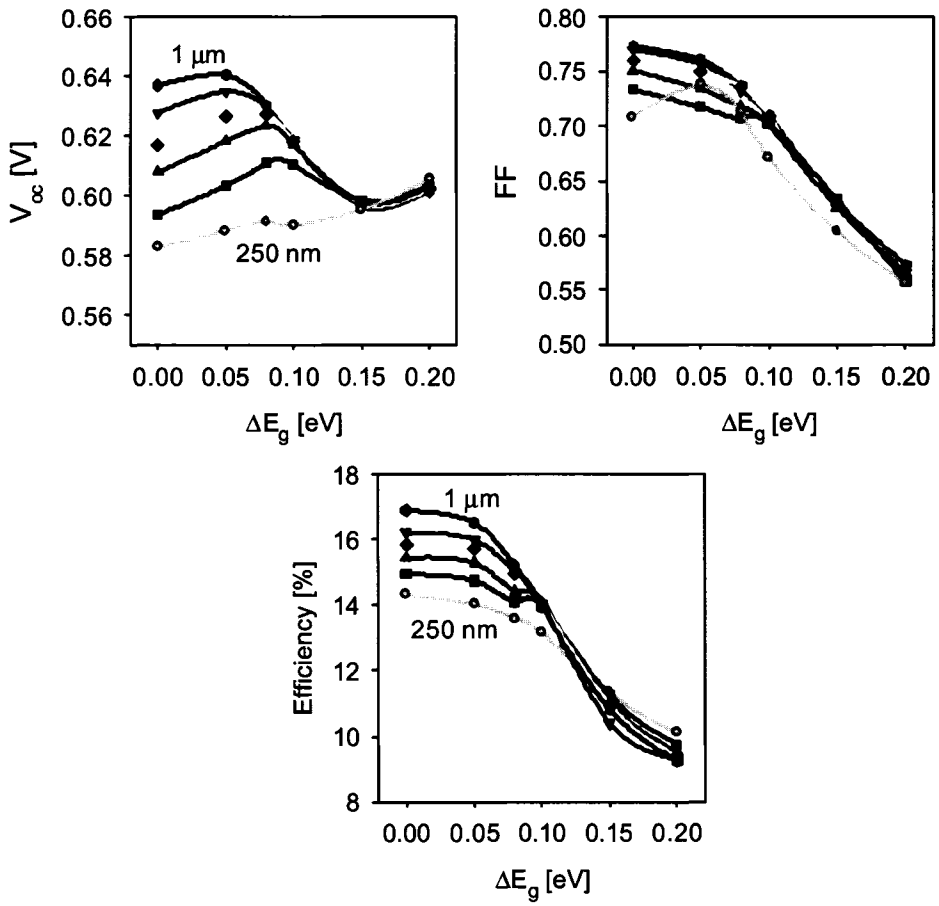

Figure 5.15. Impact of band-gap fluctuations in direction perpendicular to the junction

The hole density variation causes electrostatic fluctuations. A simulated band diagram with a hole density fluctuation amplitude of 5 is shown in Fig. 5.16. Once these potential fluctuations become large enough, the FF and the current will deteriorate.

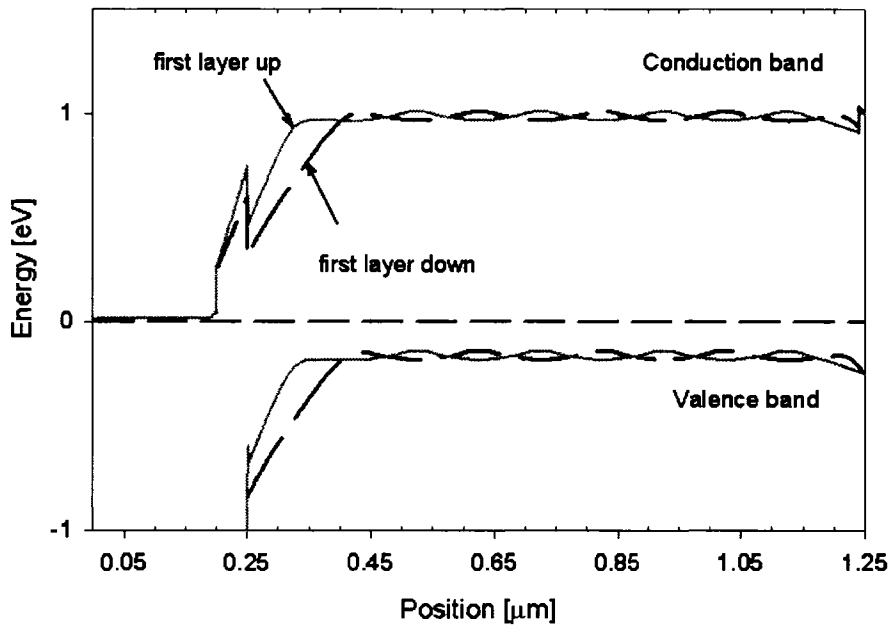

Figure 5.16. Band diagram of a 1-μm thick cell with oscillatory hole density

Figure 5.17 shows solar cell parameters as a function of the hole-density oscillation amplitude Δp. The amplitude Δp is defined as a fraction of the baseline hole-density value $p_b = 2 \times 10^{16}$ cm^{-3}. For example, amplitude of 1.2 means that the high hole density on the oscillatory function shown in Fig. 5.14 is 20% higher, and the low hole density is 20% lower than the baseline value.

Perpendicular hole-density variations will in general improve the voltage, but decrease the short-circuit current. Both the voltage improvement and current decrease are more pronounced for thinner devices. Unlike the efficiency for 1-μm or thicker devices, which is nearly independent on hole-density fluctuations, the current loss for the

thinnest device analyzed, d = 250 nm, is more pronounced than the voltage gain. This results in a 2% efficiency loss for an order of magnitude variation in hole-density.

For the 250-nm cell, there is only 1 period of oscillation within the absorber. When the first layer is up, the result on the band diagram is a barrier in the conduction band, which lowers the FF for the oscillation amplitudes between 5 and 10. In forward bias, this barrier increases. For oscillation amplitudes higher than 10, the barrier is high enough that electrons can not overcome it for any voltage bias. Therefore the losses are seen in the current as opposed to the fill-factor.

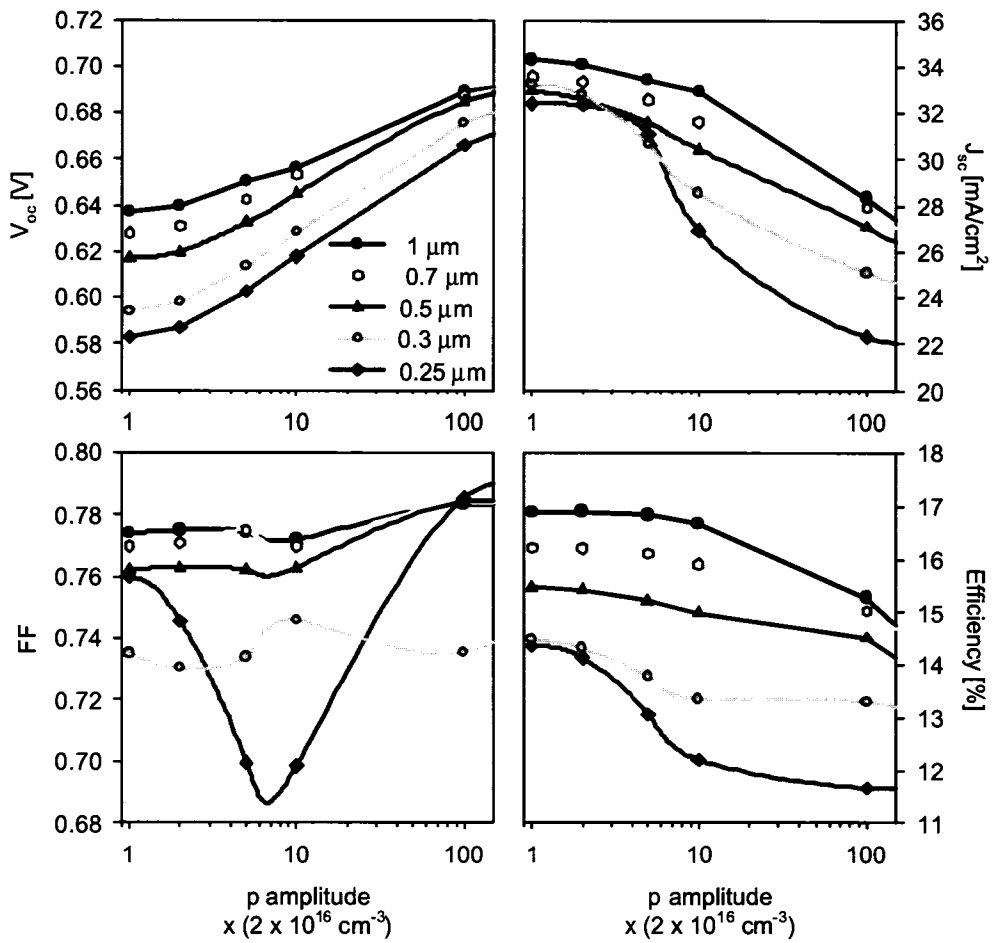

Figure 5.17. V_{oc}, J_{sc}, FF and efficiency dependence on hole-density fluctuations

The minority-carrier lifetime fluctuations have similar effect on the band diagram. Variations of lifetime for an order of magnitude or less increase the voltage, but decrease the current. The impact on efficiency is negligible (Fig. 5.18), except for the fully depleted device, which experiences efficiency decrease of ~1% due to small lifetime fluctuations. A lifetime variation of two orders of magnitude or higher decreases the voltage as well as the current. For high enough fluctuations, the efficiencies for all thicknesses converge.

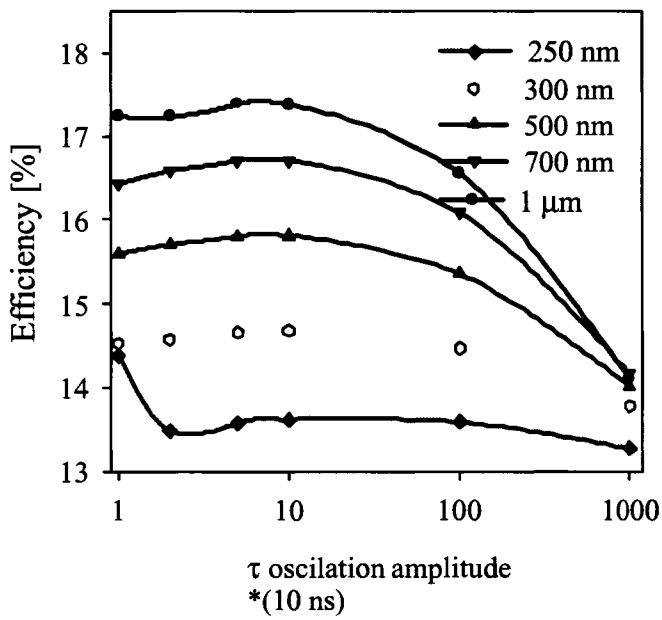

Figure 5.18. Lifetime variation impact on device efficiency

CHAPTER 6

BACK-SIDE ILLUMINATION

6.1. Motivation

Illuminating the solar cell from both sides can increase its total output per unit area. Bifacial cells based on Si have shown an improvement of 30% compared to the single-sided ones. Si cells with back-side-illumination performance comparable to the front have been fabricated over a decade ago [67-70]. Back-side illumination of CdTe solar cells has been used to investigate the back junctions and transport mechanisms [71]. In CIGS solar cells, however, due to the large absorption coefficient, back-side illumination becomes possible only when absorber is thin enough.

In addition to bifacial applications, there are situations when light enters the solar cell from the back side, and back-side illumination behavior can give valuable information. One is in tandem solar cells. In these cells, the top-cell absorber has a high band gap, thus letting the low energy part of the solar spectrum reach the bottom cell. Some of the light can be reflected from the bottom cell, and enter the top cell from the back side. In single-junction solar cells, part of the light can be reflected from the back contact and return to the absorber from the back side. If certain steps are taken to optimize the cell for back-side illumination, while not significantly compromising the front-side performance, the total output efficiency could be increased.

Thin CIGS devices with transparent back contacts produced 1.3 times higher total output power compared to the single-side illuminated when they were installed at a 30-degree angle above white concrete [72].

6.2. Primary difference between front and back illumination

A schematic of a typical CIGS solar cell with light incident from front and back side is shown in Fig. 6.1. The baseline case is equivalent to the baseline used in Chapter 4, except for substitution of the standard opaque contact with material with 85% transparency.

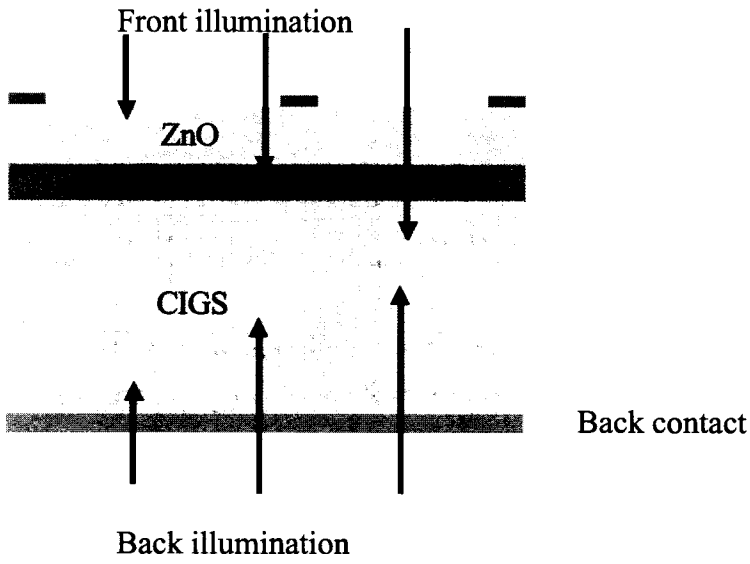

Figure 6.1. A schematic of a typical CIGS solar cell with front and back-side illumination

Unlike front illumination, where light needs to pass only through the transparent high-band-gap window and buffer layers to reach the junction region, back–side illumination requires most of the light to be absorbed in the bulk part of the absorber.

For example, for the baseline case, 83% of the electron-hole generation for the solar spectrum happens in the depletion region for front-side illumination, while only 2% for the back-side illumination. The light absorbed from the back-side illumination generates carriers in the bulk of the absorber, often far from the electric field and close to the back contact. Therefore back-illuminated solar cells require more attention towards the back contact and towards collection improvement.

Current-voltage curves for a 1-μm CIGS cell in the dark and when illuminated from the front, from the back, and simultaneously from both sides are given in Fig.

6.2. The current for back-side-illuminated device is significantly lower than for the front side. Some ways to increase the back current will be discussed below. The bifacial current is nearly equal to the sum of the front- and back-illumination currents. (It is actually slightly lower than the sum of the two, because the high carrier density generated by the front-side illumination lowers the back-illumination carriers' diffusion towards the depletion region). Since the voltages are similar, the total output power is nearly equal to the sum of the output powers for single-sided illumination. If the cell is optimized for back-side illumination, bifacial illumination can lead to significant output power increase. Note that since the total input power is no longer one sun, the definition of conversion efficiency is ambiguous and has been defined in different ways by different authors.

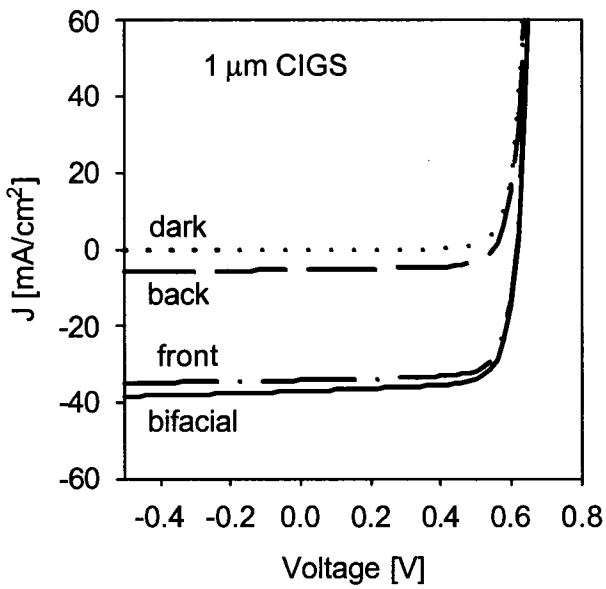

Figure 6.2. Current-voltage curves for a 1-μm CIGS cell in dark, illuminated from the front, back and simultaneously from both sides.

6.3. Back contact

The first step necessary to use a standard solar cell as a bifacial device is replacement of the opaque molybdenum with a transparent or semitransparent material. Some of the replacements for Mo that have been investigated include F-doped SnO_2 and indium-tin oxide (ITO). Both these materials show transmittance of over 85% at an incident wavelength of 550 nm and form ohmic contacts with CIGS. Additionally, $MoSe_2$ that forms on the interface between Mo and CIGS is semitransparent [49]. Transparent-back-contact cells have shown performance comparable to the standard devices. Review of the transparent-back-contact properties is given in Ref. [73-75].

When a solar cell is illuminated from the front side, the light reaches the back contact only in very thin cells. For back illumination, there is always a significant density of carriers generated close to the back contact. Therefore, if the recombination at the back contact is high, there will be significant current loss regardless of the absorber thickness. The back reflector defined in Chapter 4 has a significantly stronger impact on submicron back-illuminated cells than on front-illuminated ones. This impact is illustrated on the quantum-efficiency curves shown in Fig. 6.3. For a device with a 2-μm thick absorber (Fig. 6.3.a) the carriers generated by back illumination are very far from the electric field. Although the back reflector increases the current by 9 mA/cm^2, the quantum efficiency is still very low. Once the absorber thickness is 1 micron or lower (Fig. 6.3. b and c), the carriers are generated sufficiently close to the space-charge region. If they are not lost at the back contact, most of them will reach the junction and contribute to the current. In these cases, the back-reflector plays much more significant

role, increasing the current by 17 mA/cm^2. Note that the quantum-efficiency curves without a back-electron reflector (dashed lines in Fig. 6.3.), show significant losses for low-wavelength photons due to their lower penetration depth.

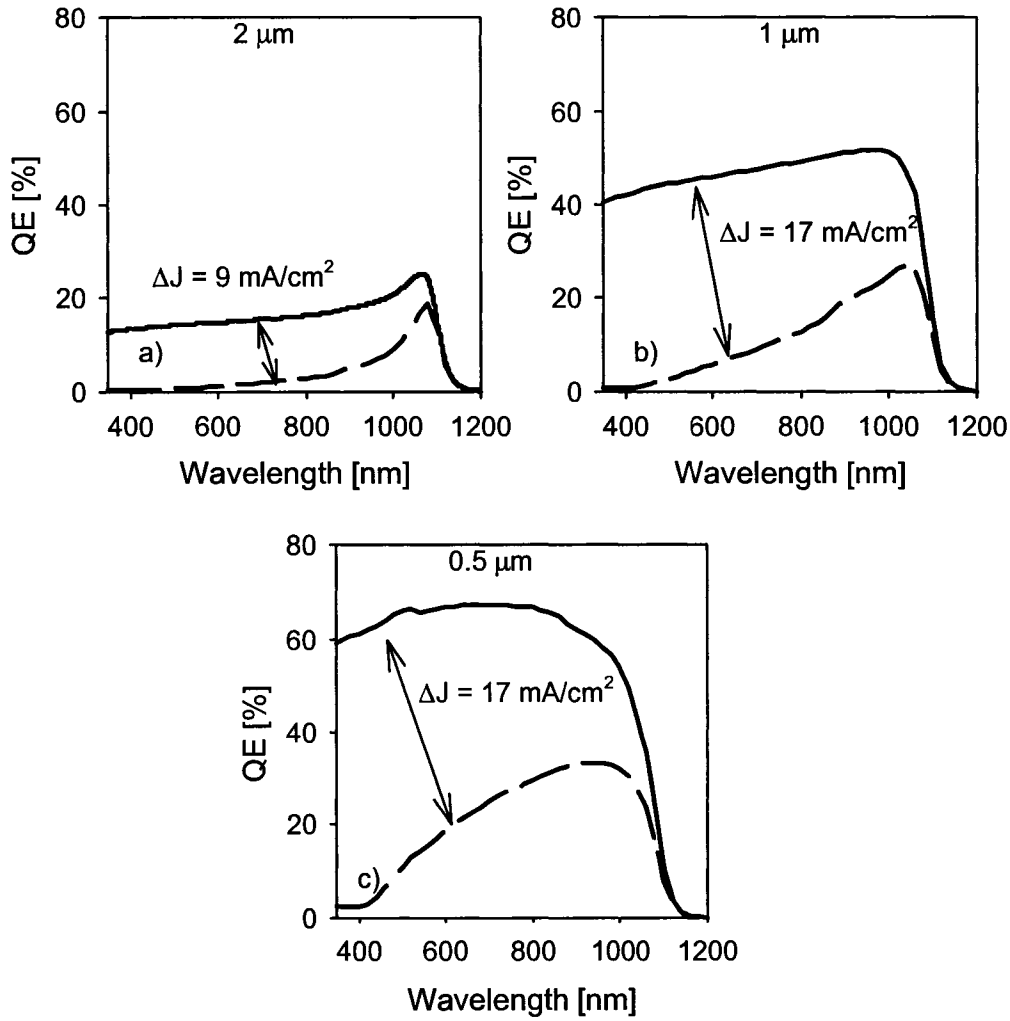

Figure 6.3. Influence of 0.2 eV high back reflectors on calculated quantum-efficiency curves for back-side illuminated devices with: a) 2-μm thick, b) 1-μm thick, and c) 0.5-μm thick absorber

6.3.1. Electron-back reflector height

The dependence of solar-cell parameters on the electron-reflector height for back illumination (filled symbols) is shown in Fig. 6. 4. The front-illumination data (open symbols) is shown for comparison. All of the parameters are improved by the electron-back reflector. The benefits for back-side illumination are stronger than for front-side illumination. Note that the front illumination parameters increase shown in Fig. 4.8 looks negligible on the much larger scale in Fig. 6.4. The benefits saturate at back reflector heights of 0.2 eV. As opposed to front illumination, where the back-reflector becomes more important for thinner devices, the back-reflector benefit for back illumination is similar for both devices. Inclusion of the back reflector lowers the difference between front and back-illumination efficiency from over 10% to approximately 4% for the 1-μm device and to about 2% for the 0.5-μm device.

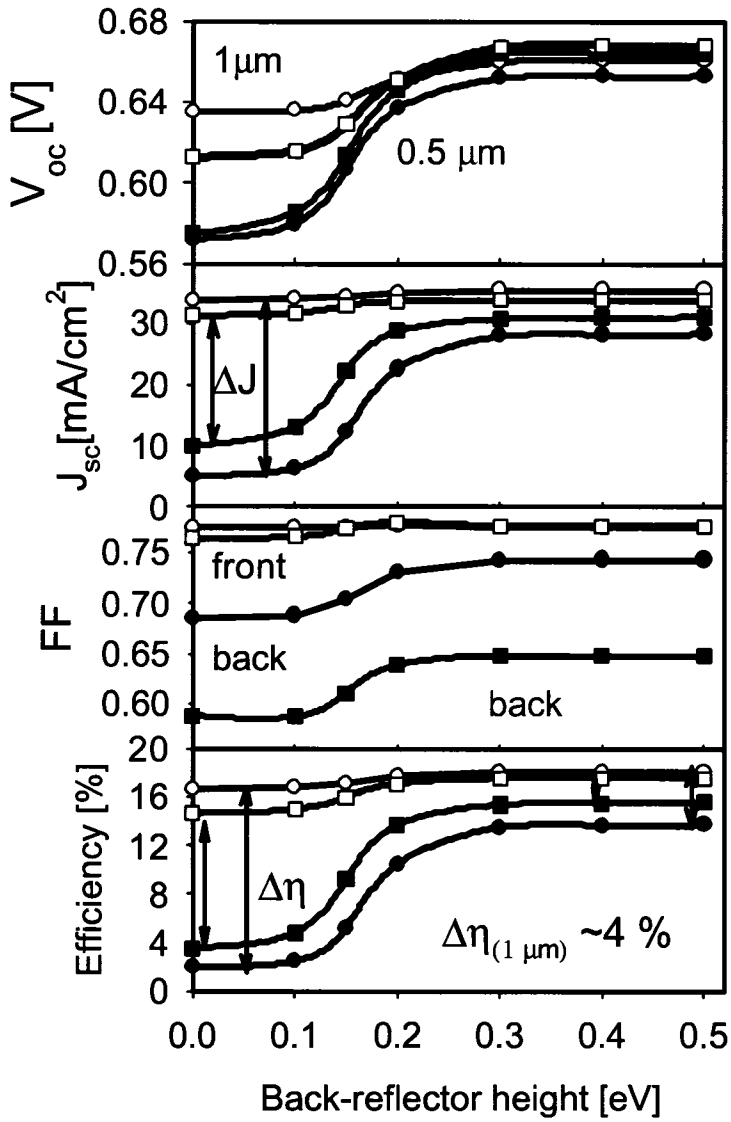

Figure 6.4. V_{oc}, J_{sc}, FF and efficiency dependence on back-reflector barrier height. $\Delta\eta$ is the front-back efficiency difference

6.4. Absorber thickness

The dependence of cell parameters on absorber thickness for back-illuminated cells is shown in Fig. 6.5. A 10-nm thick 1.35 eV back-electron reflector between the

absorber and the back contact was assumed. The front-illumination performance is also plotted for comparison. Note that due to the change in back-contact transparency, the front-illumination performance in Fig.6.5 is slightly different than the one shown in Fig. 4.2. The back-illumination current increases with thinning the absorber down to 0.5 μm. For thicknesses below 0.5 μm it follows the front-illumination current drop caused by incomplete absorption. In these calculations, the grain size was assumed to decrease at the same rate as the thickness. The experimental data from [72] (triangles in Fig. 6.5) can be fitted with this model (dashed lines in Fig. 6.5) if the minority-carrier lifetime is reduced by an order of magnitude, and the lifetime dependence on the absorber thickness is cubic.

The impact of grain boundary recombination is here incorporated as lifetime dependence on thickness. If the grain size decreases at the same rate as the absorber thickness (columnar grain boundaries), the lifetime dependence on thickness is quadratic. If the grain size decreases faster than the absorber thickness (noncolumnar grain boundaries), the grain boundary recombination can be modeled as cubic dependence of lifetime on thickness [41].

The optimal absorber thickness for this particular case is ~ 700 nm.

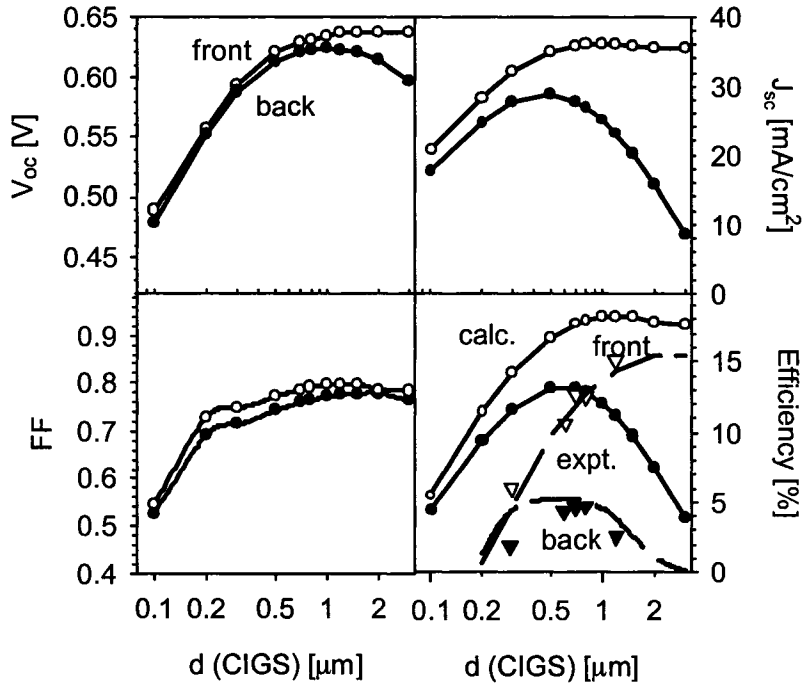

Figure 6.5. Calculated dependence of solar cell parameters on absorber thickness for back- and front-side illumination.

6.5. Carrier density

Variation in hole-density will change the space-charge-region width within the absorber. An expansion of the depletion region due to lower hole density can help the collection of back-side generated electrons.

Contour plots of the calculated cell parameters as a function of carrier density and absorber thickness are shown in Fig. 6.6. The voltage behavior is similar for the front and back-illuminated cells. The carrier density in the absorber slightly increases the open-circuit voltage. For thinner absorbers, the voltage decreases due to higher grain-boundary recombination. Higher recombination increases the forward current, and in this

way it limits the voltage. Short-circuit currents and fill-factors are, on the other hand, quite different depending on which side the light comes from. Higher doping decreases the space-charge region width, and thus for a certain absorber thickness, increases the distance from where most of the carriers are generated to the high field region. This large distance causes collection problems resulting in low currents and fill-factors for thick and highly doped devices. For fully-depleted absorbers (lower left corners on the graphs in Fig. 6.6) the performance is independent of carrier density. Unlike the front-illumination efficiency that monotonically decreases for submicron thickness, for each carrier density, the back-illumination performance has an optimal thickness, which shifts towards higher thickness for lower doping. The model predicts 14% efficiency for a back-side illuminated 1-μm thick cell, with hole density of 2×10^{15} cm^{-3} or lower. The efficiency of the same device when illuminated from the front side is ~ 16%. This modest efficiency difference shows that with appropriate optimization back-illuminated performance can be comparable to the front and can in fact nearly double the output power.

If the absorber is ~1 μm thick, and the hole density is 10^{15} cm^{-3}, the front performance efficiency is higher than 16%, and the back efficiency is 14%. This is the optimal region for bifacial illumination usage.

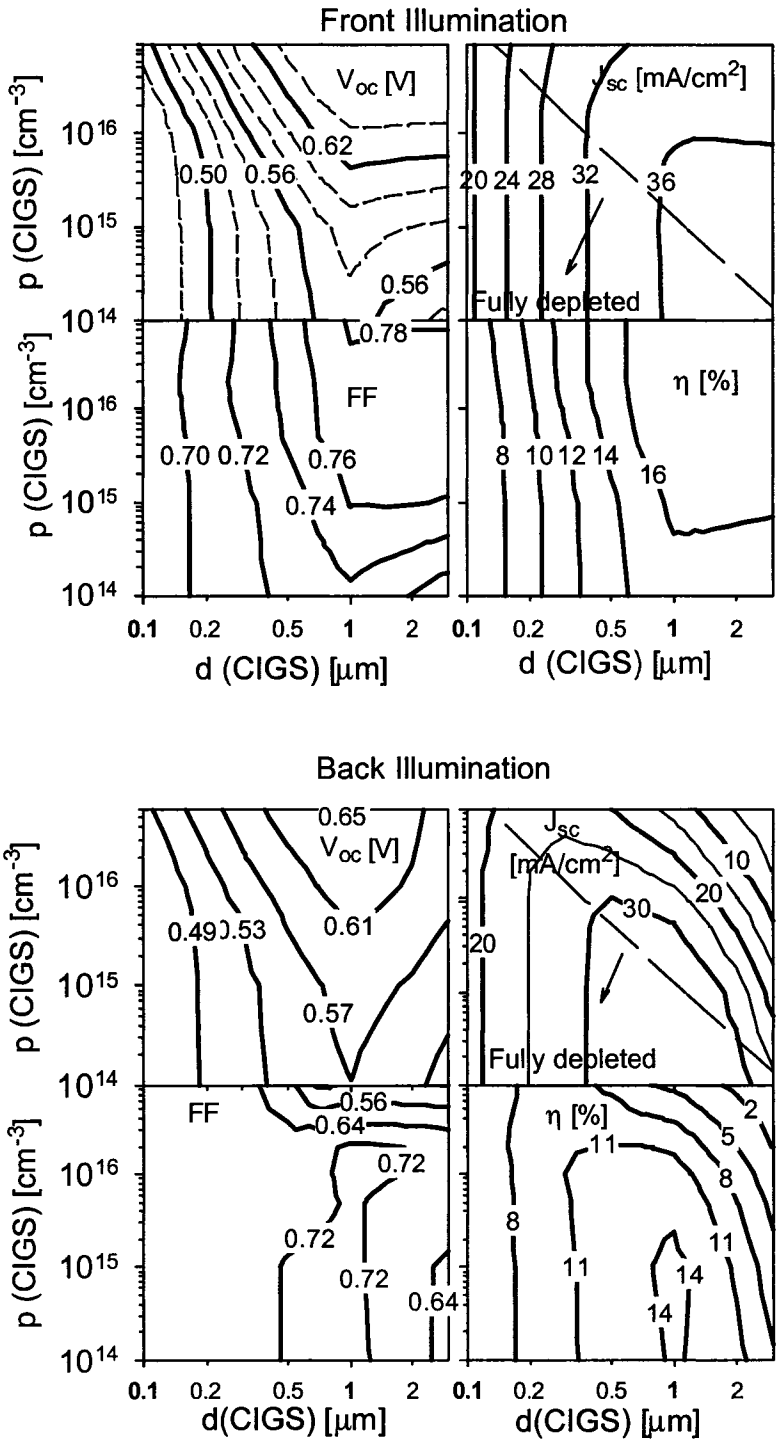

Figure 6.6. Contour plots of V_{oc}, J_{sc}, FF and efficiency as a function of absorber doping and thickness for front and back illumination. All the cases have a back-electron reflector included.

6.6. Mobility and lifetime

Since the diffusion of carriers through the bulk of the absorber is more important for back-side illumination, one would expect minority-carrier mobilities and lifetimes to affect the back-illuminated cell efficiency more strongly. Fig. 6.7.a) shows calculated results for the impact of mobility variation on the cell efficiency for a 1-μm thick (circles) and 0.5-μm thick (squares) absorber device. The mobility in fact impacts the device more strongly for back illumination than for front illumination. The effect is slightly stronger for the 1-μm thick absorber, due to the fact that the carriers need to travel further to the junction. The lifetime results are shown in Fig. 6.7.b). The back-illumination efficiency is more sensitive to the lifetime variations than to the mobility, and the lifetime impact on efficiency is stronger for thicker devices. This confirms the importance of absorber quality for back-illuminated devices.

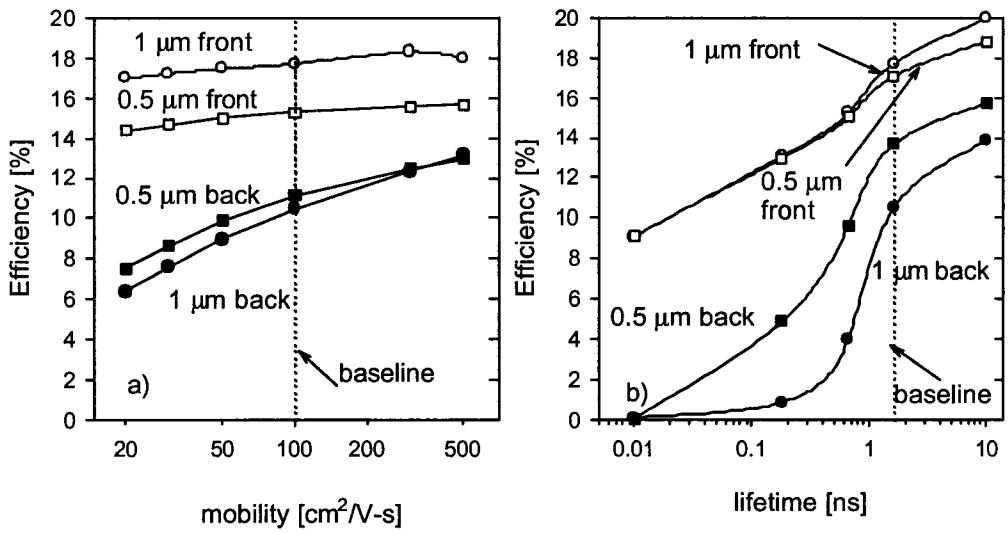

Figure 6.7. Efficiency dependence on the minority carrier a) mobility and b) lifetime, for front (open symbols) and back illumination (filled symbols)

6.7. Absorber band gap

CIGS parameter dependence on the absorber band gap has been studied extensively. Theoretically, widening of the band-gap should result in a current decrease and voltage increase. In fact, reported experimental voltages increased up to a Ga/(In+Ga) ratio of 30% and then stop following the band-gap increase. As a result, CIGS efficiency has had a maximum at band gap of 1.15-1.20 eV.

Contour plots of cell efficiency as a function of the absorber band gap are shown in Fig. 6.8. In these calculations, the experimental trends are simulated with increased defect density for high Ga content (see Section 3.2.3.2). The optimal efficiency for front illumination for submicron devices falls in the same band-gap interval between 1.1 eV and 1.2 eV as for the standard thickness devices. Wider band-gap absorbers experience current losses without voltage gain to neutralize them. This confirms the results in Ref. [39]. The optimal band gap for back-illumination is within the same interval as for the front illumination. Lower band gap absorbers have steeper absorption profile, which results in stronger carrier generation close to the back contact and severe efficiency loss. High band gap loss for back-side illumination is stronger for thicker absorbers. When a cell that has a high Ga content in the absorber is illuminated from the front side, the thinnest absorber devices suffer strongest losses.

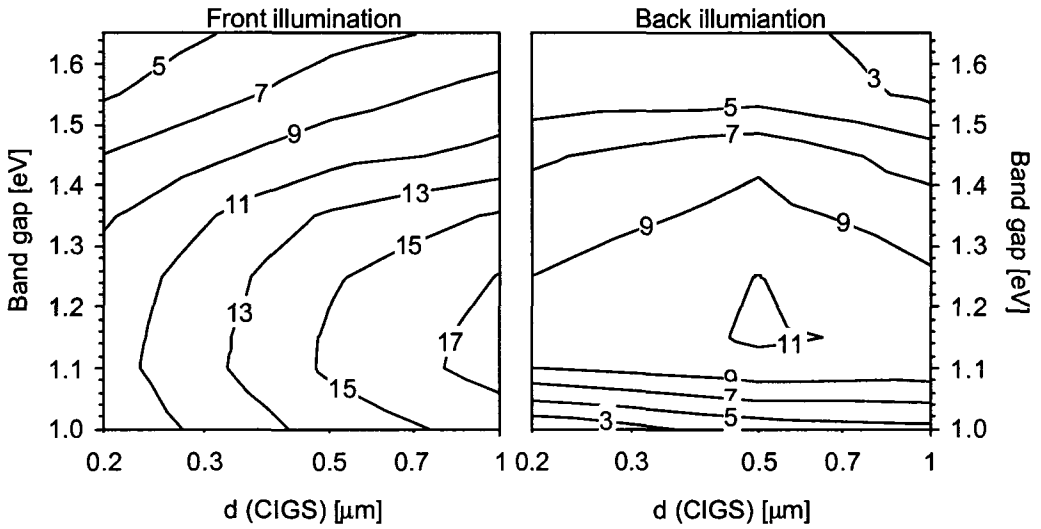

Figure 6.8. Cell efficiency as a function of absorber band gap and thickness

6.8. Band gap profile

The impact of absorber grading for front illumination has been discussed in section 4.6, and the schematic of a graded absorber is shown in Fig. 4.9. Back grading for front-side illumination predicts slight current improvements mainly due to better carrier collection [31, 34, 50, 76, 77]. For back-side illumination, however, the benefits of grading are much more intense because it not only:

a) lowers the back-contact recombination, and

b) creates electric field pushing the carriers towards the SCR, but it also

c) provides deeper generation of carriers.

There is an optimal point in the absorber where the grading should start. If the grading starts far from the SCR region, the collection is poor, which results in a FF loss. On the other hand, if the graded region has expanded far enough that it enters the depletion region, the grading has less effect for two reasons: the collection within the

depletion region is already very good (and therefore the benefit of grading is lower), and also the electric field introduced by the grading is lower. The best results were achieved for grading that starts between 50 and 150 nm outside of the depletion region. Contour plots of the impact of graded vs. constant band gap region on the cell efficiency are shown in Fig. 6.9.

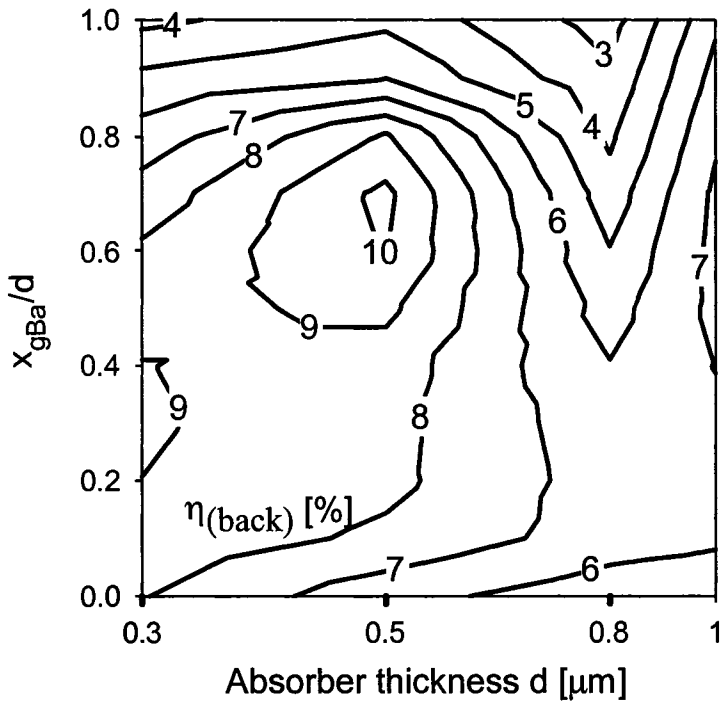

Figure 6.9. Back-side efficiency as a function of the ratio between the graded region and the absorber thickness. $\Delta E_{Ba} = 0.2$ eV

The increase of the slope of the grading ΔE_{Ba} improves the back performance up to ΔE_{Ba} of 0.3 eV, and then saturates for higher values. The saturation appears due to the balance between two effects: 1) the increase of electric field due to higher band-gap slope has a positive effect, and 2) higher defect density due to higher Ga content has a negative effect. The front-illumination performance is not significantly affected by ΔE_{Ba}.

Front grading alone has been shown to be detrimental both for front-side and for back-side illuminated cells. However, front grading as an addition to the back grading improves the voltage, since the voltage is determined by the band gap in the space-charge region. On the other hand, front grading introduces a reverse electric field, pushing carriers away from the junction. This is more detrimental for the back-side illumination. As soon as the slope towards the junction (ΔE_{fr}) becomes too large, the reverse electric field that is proportional to ΔE_{Fr} causes poor collection and fill-factor loss. There is a trade of between the voltage improvement and the fill factor loss when introducing front grading. It can be concluded that the front grading is slightly beneficial for back illumination and mainly affects the voltage, as long as it is confined within the space-charge region and the ΔE_{fr} is 0.1 eV or lower.

CHAPTER 7

ROLE OF BUFFER LAYER IN THIN DEVICES

7.1. Illumination with red photons in submicron devices

In some of the situations analyzed in previous chapters only low-energy photons – 'red photons' reach the vicinity of the p-n junction. When the solar cell is illuminated from the back side, for example, because of the higher penetration depth of the low-energy photons, only they will reach the p-n junction and be collected. If in submicron devices, the back contact has high reflectivity, the reflected light will mainly consist of high-wavelength photons. In tandem cells, which have gained considerable interest in the recent years, the light reaching the bottom junction is partially or fully depleted of high-energy photons. Therefore, studying the behavior of a CIGS solar cell that is only illuminated with red photons is of special interest.

7.2. Red-light distortion

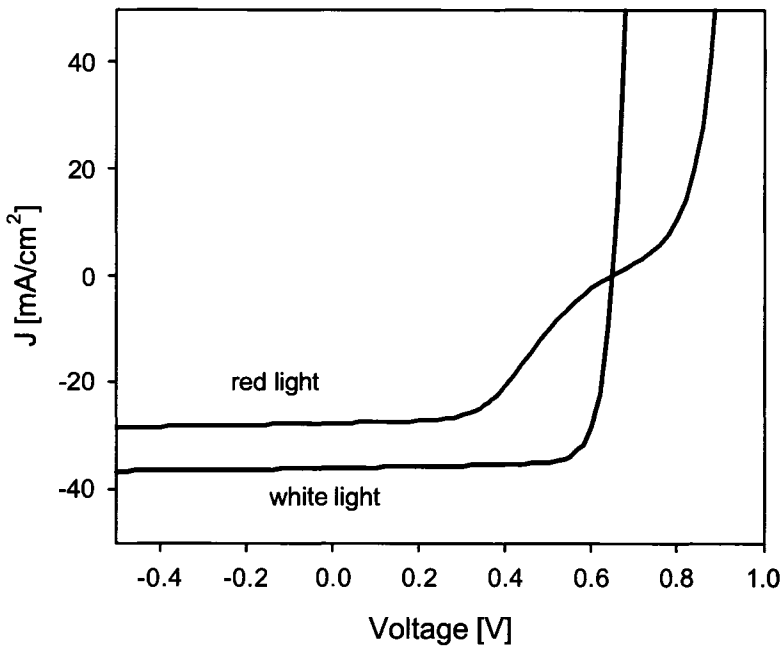

Figure 7.1. Current-voltage curves of a 1-μm thick cell illuminated with red and white light.

When a ZnO/CdS/CIGS cell is illuminated only with photons that have energies lower than 2.4 eV, which corresponds to the band gap of CdS, the current-voltage curve can be significantly distorted from the standard exponential curve. The distortion, often referred to as "red kink", has been observed in CdS/CIS cells and in CIGS cells with low Ga content [30, 78-84]. Fig. 7.1 shows simulated J-V curves with full spectrum present-white light, and only with illumination above 520 nm– red light. Experimental red-light curves are often similar.

The conduction-band offset between CIGS and CdS is positive (Fig. 7.2) and often referred to as "spike". For the optimal Ga/(In+Ga) ratio of 30%, it is approximately

equal to 0.3 eV [19]. This offset creates a secondary barrier for the light-generated electrons. When the cell has been exposed to high-energy photons, photoconductivity of CdS will lower the effective barrier, and the distortion disappears. The conduction band for a cell illuminated with red light only, and with white light is shown in Fig. 7.2. The time for recovery of the J-V curve varies from cell to cell, but it typically ranges from several seconds to a few minutes. After the cell has been in dark, the distortion gradually reappears, usually on a time scale of hours.

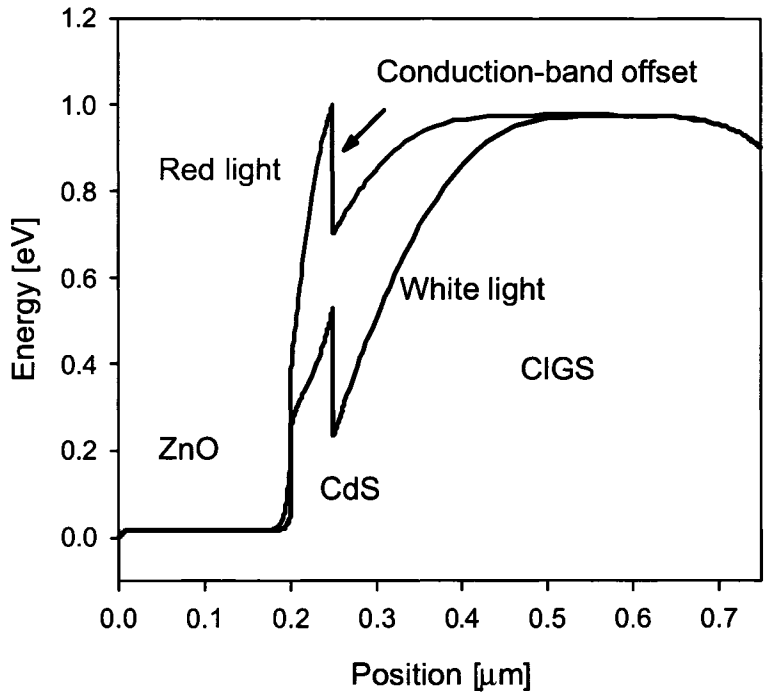

Figure 7.2. A conduction band for a 0.5-μm thick cell illuminated only with red light and with white light.

7.2.1. The mechanism behind the distortion

The electron-current density in direction of transport x can be calculated as [85]:

$$J_n = q\int_{E_c}^{\infty} v_x dn \tag{7.1}$$

If one assumes thermionic emission across the interface between CIGS and CdS, then the electron velocity is approximately equal to the thermal velocity $v_{th} \approx 10^7 cm/s$.

$$J_n = qnv_{th} \tag{7.2}$$

The electron density n can be calculated from:

$$n = N_c \exp\left(-\frac{E_c - E_{Fn}}{kT}\right) \tag{7.3}$$

where N_c is effective density of states in the conduction band, E_c is the conduction-band minimum energy, and E_{Fn} is the energy of quasi-Fermi level for electrons. The maximum current that can flow through the junction is limited by the electron-density in the CdS at the interface with CIGS. This can be determined with a distance between the Fermi level and the conduction-band minimum. If one assumes that the light-generated current is J_{sc} = 28 mA/cm^2, the minimal density of carriers needed to provide this current is 1.75 x 10^{10} cm^{-3}, and thus the energy difference between the conduction-band minimum and the quasi-Fermi level for electrons, calculated from equation (7.3) needs to be lower than 0.48 eV. This rule applies to various situations in which red-light distortion is present, though it needs to be modified slightly for different current densities. The validity of the 0.48-eV rule for variations of CdS thickness, defect-density in CdS, and the conduction-band offset between CIGS and CdS was shown in Ref. [86].

7.2.2. Kink in thin vs. thick devices

Figure 7.3 shows the effect of defect-density variation in CdS on a 'red' current-voltage curve for a 1-μm thick device, a 500-nm thick device, and a 250-nm thick device. When the blue photons are removed from the solar spectrum, the intensity is about 60% of the total intensity and therefore, the short-circuit current for red-light illumination is lower than the white-light illumination current. Since the red-light distortion is a feature of CdS layer, one might expect it to not be affected by absorber thickness. This is generally the case in Fig. 7.3. In case 7.3.c), however, when the device is fully depleted, the current reduction in red light is slightly more severe. In the white light, there is no change in the J-V curve as a result of CdS defect-density variation at any of the thicknesses shown.

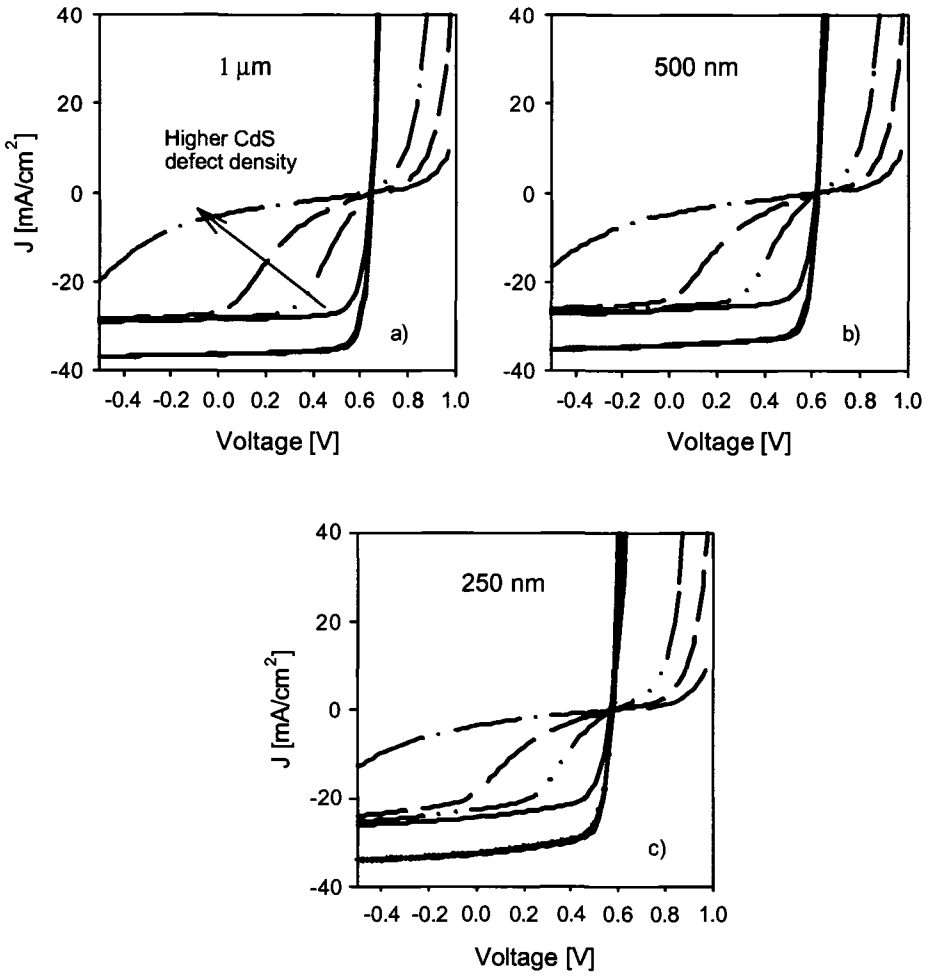

Figure 7.3. Calculated red and white current-voltage curves for a) 1-μm thick device, b) 500 nm and c) 250 nm.

The energy difference between E_c and E_{Fn} at zero voltage bias as a function of position is shown in Fig. 7.4. The defect densities are the same as in Fig. 7.3. The defect density in CdS ranges from 10^{17} (black curve) to 5 x 10^{17} cm^{-3} (green). At zero bias, the highest defect density curve (green line) shows significant current reduction. The E_c - E_{Fn} level for this defect density is well above the 0.48 eV value. The next curve (blue) shows slight reduction at 0 V, and both E_c - E_{Fn} values are slightly above the 0.48 eV value. It can be concluded that the 0.48 eV-rule applies equally to thin devices as to thick ones,

and hence the red-light distortion is nearly equally pronounced at devices with different thicknesses.

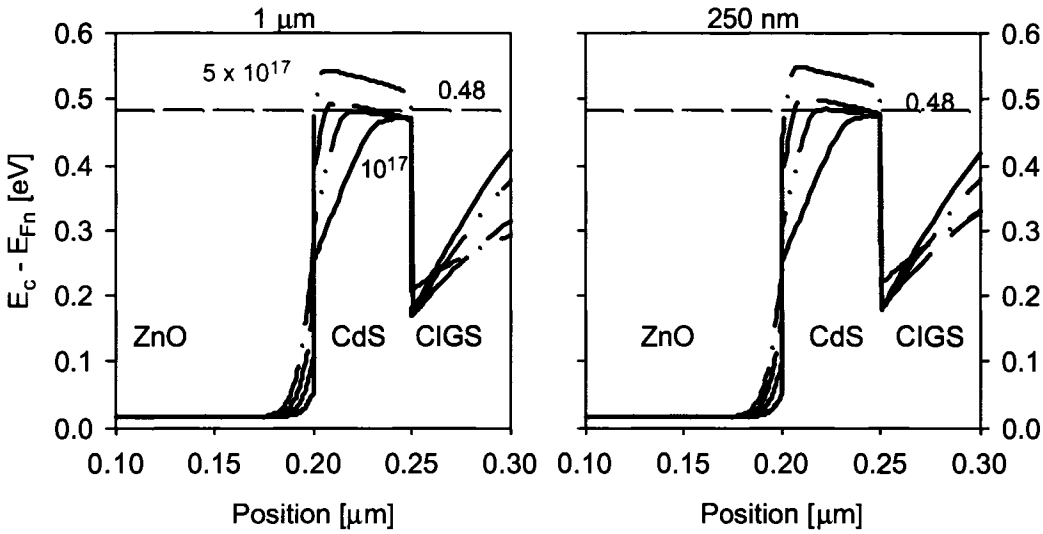

Figure 7.4. E_c-E_{Fn} for a 1-μm and 250-nm thick device. The four curves represent different defect densities in CdS.

7.3. Alternative buffer layers

In addition to possibly causing the red-light distortion, the CdS layer has an additional disadvantage of lowering the overall current in the low-wavelength region. As discussed in Chapters 4 and 6, the current loss is the biggest problem in submicron devices and back-illuminated CIGS cells. Additional loss in the CdS layer compounds the problem.

If CdS was substituted with a higher-band gap layer, more photons would reach the absorber, and contribute to the total current. Solar cells with complete elimination of CdS, however, in general perform worse then the ones with a buffer layer [87].

Choosing the alternative buffer layer is a complex task. Some of the criteria are listed in 2.3.3. An additional demand from a buffer layer is to have an appropriate band offset with CIGS. Two alternative buffer layer materials, $Mg_xZn_{1-x}O$, and $Cd_xZn_{1-x}S$ are investigated below.

7.3.1. $Mg_xZn_{1-x}O$

The conduction-band offset as a function of Mg content in the compound has been calculated by Minemoto et al. [88, 89].

Experimental efficiencies of cells deposited by Falah Hasson from the National Renewable Energy Laboratory are shown in Fig. 7.5 with filled circles. Simulation results of the cell efficiency that match the experimental data are given with open squares. The efficiencies obtained by $Mg_xZn_{1-x}O$ cells were up to 95% of the equivalent CdS cell [90]. Calculations have confirmed that, for an absorber with a band gap of 1.15 eV, there is an optimal Mg content between 10 and 20 %, corresponding to conduction-band offsets of 0.1 to 0.35 eV. For lower Mg contents, (Region 1 in Fig. 7.5) for no band-offsets, or negative band offsets "cliffs", there is a voltage loss due to recombination at the interface, and the efficiency is decreased. In Region 3, the band-offset creates a very high barrier for the generated electrons, resulting in major current loss and again low efficiency. Variation in Ga content in CIGS will change the conduction-band offset between CIGS and $Mg_xZn_{1-x}O$. Wider band-gap devices will need a buffer with higher Mg content.

The rule that negative conduction-band offset limits the voltage, and large spike limits the current, can be applied for buffer layers in general.

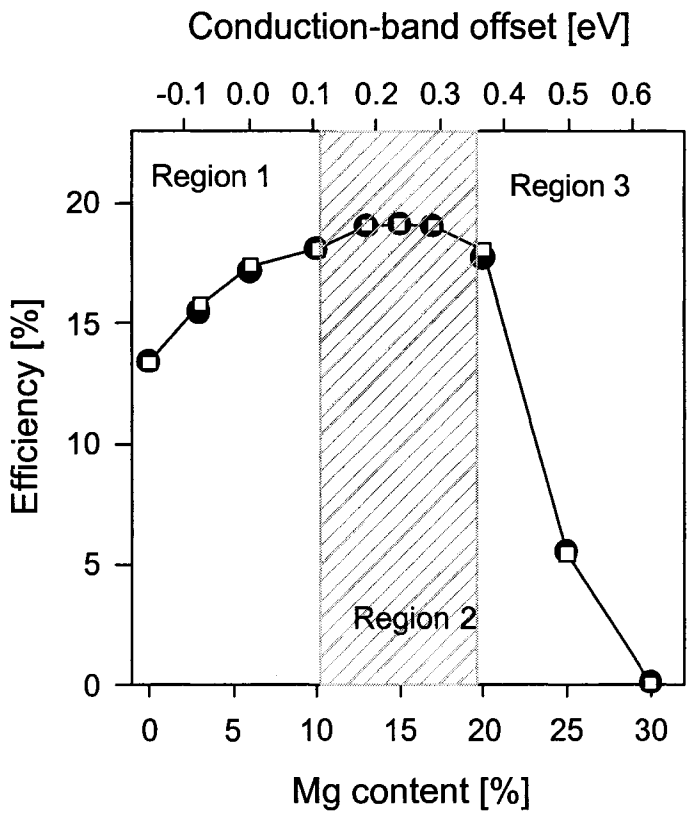

Figure 7.5. The efficiency of $Mg_xZn_{1-x}O$/CIGS solar cell as a function of Mg content x

7.3.2. $Cd_xZn_{1-x}S$

The most successful CdS replacements in the past were ZnS(O,OH) that achieved 18.5% efficiency [91], and CdZnS with 18.6% efficiency [92]. Recently, however, a CdZnS device with efficiency equal to the record CdS device was produced by R. Bhattacharya *et al.* [9]. The ratio between Cd and Zn in this device is 80:20. In analysis of the cell, a device with a standard CdS layer with an equivalent absorber was measured for comparison. As expected, the CdZnS showed a current gain of 2 mA/cm^2 in the short-wavelength region, but 0.5 mA/cm^2 lower long wavelength collection.

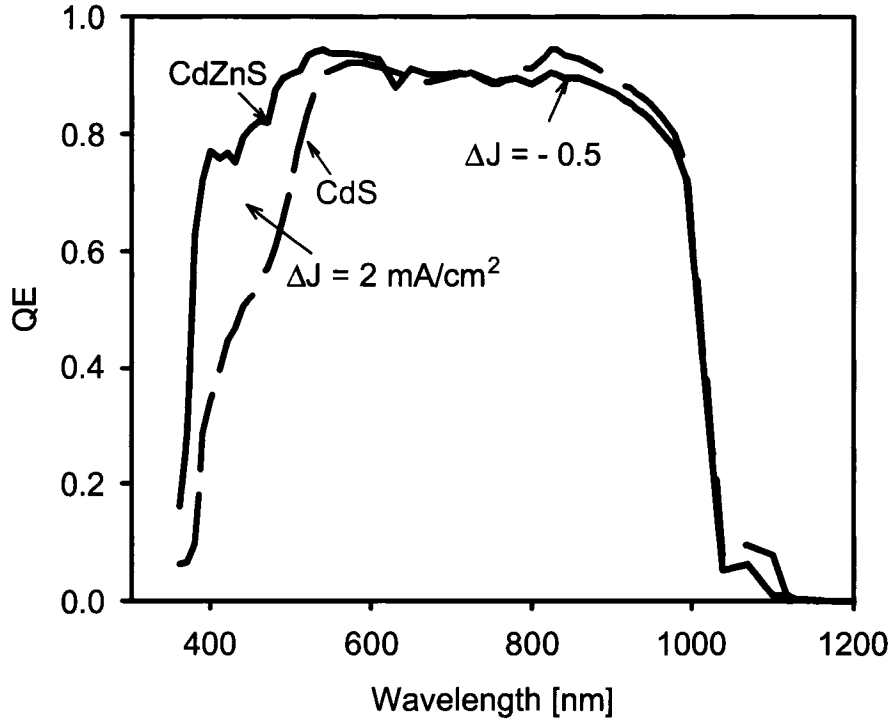

Figure 7.6. External quantum efficiency curves for a CdZnS device and a CdS with equivalent absorbers

In addition to the current gain, the alternative-buffer device showed slightly higher voltage (20 mV). The fill factor, however, was lower than in CdS device. The reason probably lies in additional defects that are present close to the junction when CdZnS is deposited. The presence of these defects can be deduced from capacitance-frequency as well as from capacitance-voltage curves. The capacitance vs. frequency curves are shown in Fig. 7.7. In reverse bias both devices are reasonably frequency independent, but at zero bias and low forward bias, the CdZnS shows a significant variation of capacitance with frequency.

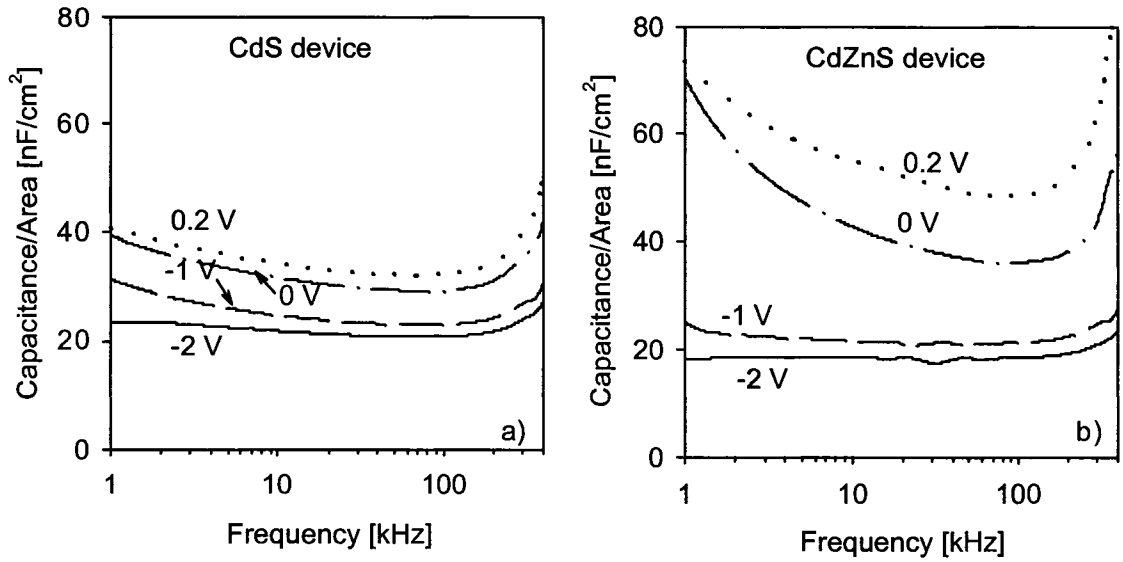

Figure 7.7. Capacitance-frequency dependence for a)CdS device compared to b)CdZnS device

The capacitance-voltage curves for the same two cells are shown in Fig. 7.8. In contrast to the capacitance-voltage curve for CdS/CIGS cell that has a linear C^{-2} vs. V dependence, the capacitance dependence on voltage for $Cd_xZn_{1-x}S$ cell is not linear, and the variation of capacitance with voltage is stronger.

Independent of the increased FF loss, the current and the voltage gain improve the efficiency of the device with the CdZnS buffer layer. Thus there is reason to believe that CdZnS/CIGS has a potential to surpass the 20%-efficiency milestone for thin-film cells in the near future.

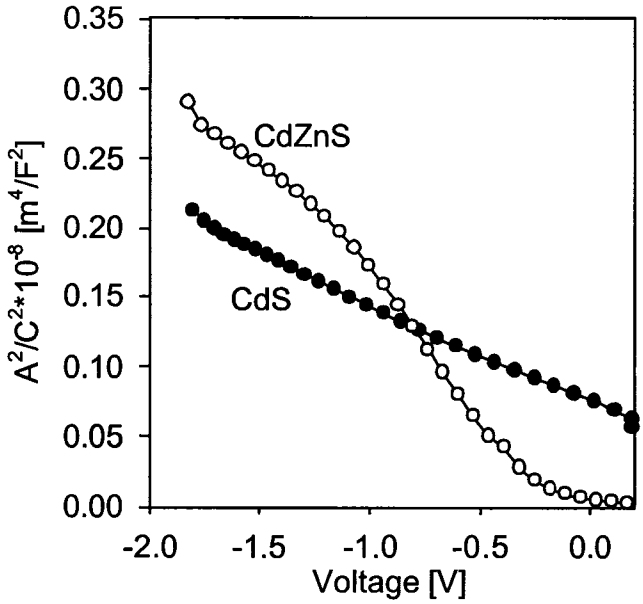

Figure 7.8. Capacitance-voltage curves for CdS and CdZnS solar cells

CHAPTER 8

CONCLUSIONS

This thesis mainly presents calculation results with the goal to provide insight to the device physics of CIGS solar cells with submicron absorbers.

For thin absorber devices, the back-contact material becomes much more important. Back-contact recombination can be lowered either by increasing the Ga content towards the back or by forming a $MoSe_2$ layer. Increased Ga at the back improves the collection, but an excessive amount of Ga increases the defect densities. The optimal thickness of the band-gap graded region is slightly lower than the quasi-neutral region, and its optimal conduction-band energy is about 0.3 eV above the minimum of the absorber bulk.

As submicron devices are more sensitive to thickness fluctuations, smoothness also becomes more important in thin absorber limit. The impact of band-gap variations

between different grains of the absorber, however, will deteriorate the performance of thin and thick devices nearly equally. Areas with lower lifetime are less detrimental for submicron devices than for the thicker ones.

A small area with lower voltage then the rest of the cell can seriously impact the entire cell performance. The voltage of a nonuniform cell will decrease linearly with the voltage of the weak region, and logarithmically with its area. Resistance in the transparent conductive oxide is useful to prevent leakage and to localize the weak area and prevent it from dominating the entire device. High resistance, however, does reduce the overall fill-factor and hence reduces the net device performance.

There is an opportunity to obtain a non-negligible output-power increase when submicron cells are illuminated from both sides. Standard absorbers with thickness of ~2 μm and constant band gap show a very low improvement with bifacial illumination. Cells thinner than a micron, however, when optimized for bifacial illumination, can produce efficiencies with back illumination comparable to front illumination.

Calculations have shown that with back illumination one needs to pay much stronger attention to bulk quality and that it is crucial to provide a back-electron reflector. There is an optimal absorber thickness for back-side illumination that depends on the hole density. Devices thicker than the optimal experience current loss, while devices thinner than optimal experience voltage loss. Lower doping expands the space-charge region and loosens the bulk quality requirements. Band-gap grading is beneficial for absorbers with high defect densities, where it can substantially improve the collection.

Although CdS has been widely used as a buffer layer between the ZnO and CIGS, it may not be the optimal solution. A long-going search for alternative, wider-bang gap

and cheap alternatives has led to CdZnS that improves the short-circuit current and has a potential to soon overcome 20%.

Tandem devices, as well as submicron devices, may be the next generation of photovoltaic devices. Some of the calculations in this thesis are applicable to tandem cells. The benefits of thinning the absorbers in both cells of the tandem device are obvious, but attention must be paid to the top device, which will likely be exposed to back-side illumination reflected from the bottom cell, and the bottom cell which likely will be exposed to almost entirely red-light illumination.

The global energy problem will not solve itself. It requires combined efforts by many of us. By analyzing different aspects of submicron CIGS cells, the author of this thesis hopes to make a small contribution towards better understanding of the device physics behind them. Better understanding should lead to their wider production and usage, which will make this world a better and cleaner place.

BIBLIOGRAPHY:

[1] R. Shinnar and F. Citro, *Science* **313**, 1243 (2006).

[2] Solar Energy International: URL:http://www.solarenergy.org/resources/energyfacts.html

[3] Ken Zwiebel, The terawatt challenge for thin-film PV, NREL/TP-520-38350 2005

[4] D. M. Chapin, C. S. Fuller and G. L. Pearson, *J Appl Phys* **25**, 676 (1954).

[5] A. Luque and S. Hegedus, *Handbook of Photovoltaic Energy Conversion and Engineering*: John Wiley & Sons LTD, Chichester, West Sussex, England, (2003).

[6] M. A. Green, K. Emery, D. L. King, Y. Hishikawa and W. Warta, *Prog. Photovoltaics* **15**, 35 (2007).

[7] A. Lique and S. Hegedus, *Handbook of Photovoltaic Energy Conversion and Engineering*: John Wiley & Sons LTD, Chichester, West Sussex, England, (2003).

[8] M. A. Contreras, K. Ramanathan, J. AbuShama, F. Hasoon, D. L. Young, B. Egaas and R. Noufi, *Prog. Photovoltaics* **13**, 209 (2005).

[9] R. N. Bhattacharya, M. A. Contreras, B. Egaas, R. N. Noufi, A. Kanevce and J. R. Sites, *Appl. Phys. Lett.* **89**, 253503 (2006).

[10] National Renewable Energy Laboratory: *Will we have enough material for energy significant PV production?*, URL: http://www.nrel.gov/docs/fy04osti/35098.pdf

[11] G. Hanna, A. Jasenek, U. Rau and H. W. Schock, *Thin Solid Films* **387**, 71 (2001).

[12] R. Noufi and K. Zwiebel, in Proc. 4^{th} *WCPEC*,(2006) pp.317

[13] American society for testing and materials, Standard for Terrestrial Direct Normal Solar Spectral Irradiance tables for air Mass 1.5, West Conshocken, PA, USA

[14] Martin A. Green: Prentice-Hall, (1982), p. 80.

[15] S.M. Sze, *Physics of Semiconductor devices*, 2^{nd} ed: John Wiley&Sons, (1981).

[16] W. Shockley and H. J. Queisser, *J Appl Phys* **32**, 510 (1961).

[17] R. Noufi, R. Axton, C. Herrington and S. K. Deb, *Appl Phys Lett* **45**, 668 (1984).

[18] A. O. Pudov, *PhD Thesis*, Colorado State University (2005)

[19] S. H. Wei and A. Zunger, *Appl Phys Lett* **63**, 2549 (1993).

[20] S.S. Hegedus and W.N. Shafarman, *Prog. Photovolt: Res. Appl* **12**, 155 (2004).

[21] Martin A. Green, *Solar Cells*: the Prentice Hall, (1982).

[22] P.H. Mauk, H. Tavakolian and J. R. Sites, *IEEE Transactions on Electronic Devices* **37**, 422 (1990).

[23] M. Burgelman, J. Verschraegen, S. Degrave and P. Nollet, *Prog Photovoltaics* **12**, 143 (2004).

[24] A. Niemegeers and M. Burgelman, in Proc. *25nd IEEE Photovoltaic Spec. Conf.*,(1996) pp. 901

[25] M. Burgelman, P. Nollet and S. Degrave, *Thin Solid Films* **361**, 527 (2000).

[26] A manual for AMPS-1D for Windows'95/NT, Pennsylvania State University, (1997)

[27] M.Gloeckler, A.L.Fahrenbuch and and J.R. Sites, in Proc. *3rd WCPEC*,(2003) pp.491

[28] P. D. Paulson, R. W. Birkmire and W. N. Shafarman, *J Appl Phys* **94**, 879 (2003).

[29] M. Gloeckler, *PhD thesis*, Colorado State University (2005) http://www.physics.colostate.edu/groups/photovoltaic/PDFs/MGloeckler_Thesis.pdf

[30] I. L. Eisgruber, J. E. Granata, J. R. Sites, J. Hou and J. Kessler, *Solar Energy Materials and Solar Cells* **53**, 367 (1998).

[31] O. Lundberg, *PhD Thesis*, Uppsala University (2003)

[32] T. Negami, S. Nishiwaki, Y. Hashimoto, N. Kohara and T. Wada, in Proc. *2nd WCPEC*,(1998) pp.1181

[33] R. W. Birkmire W.N. Shafarman, S.Marsilac, M. Marudachalam, N. Orbey, and T. Russel, in Proc. *26th IEEE PVSC*,(1997) pp.331

[34] O. Lundberg, M. Bodegard, J. Malmstrom and L. Stolt, *Prog. Photovoltaics* **11**, 77 (2003).

[35] K. Ramanathan, J.C. Keane, B. To, R.G. Dhere and and R. Noufi, in *20th Eu PVSEC*, (2005).

[36] R. Noufi K. Ramanathan , B. To, D.L. Young, R. Bhattacharya, M. A. Contreras, R.G. Dhere, and G. Teeter, in Proc. *4-th WCPEC*,(2006) pp.380

[37] T. Nakada, Y. Kanda, S. Kijima, Y. Komiya, D.Ohmori, H. Ishizaki and N.Yamada, in Proc. *20th Eu. PVSEC*
(2005) pp.1736

[38] U. Malm, M. Edoff and L. Stolt, in Proc. *19th European Photovoltaic Solar Energy Conference*,(2004) pp.1890

[39] M. Gloeckler and J. R. Sites, *J Appl Phys* **98**, 103703 (2005).

[40] V.G. Karpov, M. L.Cooray and D. Shvydka, *Appl Phys Lett* **89**, 163518 (2006).

[41] M. Gloeckler, W. K. Metzger and J. R. Sites, *J Appl Phys* **98** (2005).

[42] M. A. Green, *Solid State Electron* **21**, 1139 (1978).

[43] T. Kohara T. Wada, N.Negami, T.Nishitani, M., *Jpn J Appl Phys 2* **35**, L1253 (1996).

[44] K. Orgassa, H. W. Schock and J. H. Werner, *Thin Solid Films* **431**, 387 (2003).

[45] Kay Orgassa, *PhD thesis*, University of Stuttgart (2004)

[46] S. H. Wei, S. B. Zhang and A. Zunger, *Appl Phys Lett* **72**, 3199 (1998).

[47] S. Nishiwaki, N. Kohara, T. Negami and T. Wada, *Jpn J Appl Phys 2* **37**, L71 (1998).

[48] P. J. Rostan, J. Mattheis, G. Bilger, U. Rau and J. H. Werner, *Thin Solid Films* **480**, 67 (2005).

[49] R. Coehoorn, C. Haas and R. A. Degroot, *Phys Rev B* **35**, 6203 (1987).

[50] M. Gloeckler and J. R. Sites, *J Phys Chem Solids* **66**, 1891 (2005).

[51] O. Lundberg, M. Edoff and L. Stolt, *Thin Solid Films* **480**, 520 (2005).

[52] K. Ramanathan, M. A. Contreras, C. L. Perkins, S. Asher, F. S. Hasoon, J. Keane, D. Young, M. Romero, W. Metzger, R. Noufi, J. Ward and A. Duda, *Prog Photovoltaics*
Prog Photovoltaics **11**, 225 (2003).

[53] A. J. Madenach and J. H. Werner, *Phys Rev B* **38**, 13150 (1988).

[54] V. G. Karpov, A. D. Compaan and D. Shvydka, *Phys. Rev. B* **69**, 045325 (2004).

[55] V. G. Karpov, A. D. Compaan and D. Shvydka, *Appl. Phys. Lett.* **80**, 4256 (2002).

[56] V. G. Karpov, G. Rich, A. V. Subashiev and G. Dorer, *J Appl Phys* **89**, 4975 (2001).

[57] V.G. Karpov, A. D. Compaan and D. Shvydka, in Proc. *29th IEEE PVSC*,(2002) pp.708

[58] V.G. Karpov, R. Harju and G. Dorer, in Proc. *28th IEEE PVSC*,(2000) pp.547

[59] J. H. Werner, J. Mattheis and U. Rau, *Thin Solid Films* **480**, 399 (2005).

[60] U. Rau, P. O. Grabitz and J. H. Werner, *Appl. Phys. Lett.* **85**, 6010 (2004).

[61] P. O. Grabitz, U. Rau and J. H. Werner, *Thin Solid Films* **487**, 14 (2005).

[62] P. O. Grabitz, U. Rau and J. H. Werner, *Phys. Status. Solidi A* **202**, 2920 (2005).

[63] Nishiwaki S. Hashimoto Y Negami T, Kohara N, and Wada T, in *2nd WCPEC.* Vienna, Austria, (1998), p. 1181.

[64] K. Ramanathan, R. Noufi, B. To, D.L. Young, R. Bhattacharya, M. A. Contreras, R.G. Dhere and G. Teeter, in Proc. *4th WCPEC*,(2006) pp.380

[65] Martin A. Green: Prentice-Hall, (1982), p. 145.

[66] Ingrid L. Eisgruber, *PhD. Thesis*, Colorado State University (1996)

[67] A. Moehlecke, I. Zanesco and A. Luque, in Proc. *1st WCPEC*,(1994) pp.1663

[68] A. Hubner, A. G. Aberle and R. Hezel, in Proc. *14th Eu. PVSEC*,(1997) pp.92

[69] S. W. Glunz, J. Knobloch, D. Biro and W. Wettling, in Proc. *14th Eu. PVSEC*,(1997) pp.392

[70] C. del Canizo, A. Moehlecke, I. Zanesco and A. Luque, *IEEE Electr Device L* **21**, 179 (2000).

[71] D. Desai, S. Hegedus, B. Mccandless, R. Birkmire, K. Dobson and D. Ryan, in Proc. *4th WCPEC*,(2006) pp. 368

[72] T. Nakada, Y. Kanda, S. Kijima, Y. Komiya, D.Ohmori, H. Ishizaki and N. Yamada, in Proc. *20th Eu PVSEC*,(2005) pp.1736

[73] T. Nakada, *Thin Solid Films* **480**, 419 (2005).

[74] T. Nakada, Y. Hirabayashi and T. Tokado, *Jpn J Appl Phys 2* **41**, L1209 (2002).

[75] T. Nakada, Y. Hirabayashi, T. Tokado, D. Ohmori and T. Mise, *Sol Energy* **77**, 739 (2004).

[76] A. M. Gabor, J. R. Tuttle, M. H. Bode, A. Franz, A. L. Tennant, M. A. Contreras, R. Noufi, D. G. Jensen and A. M. Hermann, *Sol Energ Mat Sol C* **41-2**, 247 (1996).

[77] M. Topic, F. Smole and J. Furlan, *J Appl Phys* **79**, 8537 (1996).

[78] M. Igalson, M. Bodegard and L. Stolt, *Sol Energ Mat Sol C* **80**, 195 (2003).

[79] A. O. Pudov, A. Kanevce, H. A. Al-Thani, J. R. Sites and F. S. Hasoon, *J Appl Phys* **97** (2005).

[80] A. O. Pudov, J. R. Sites, M. A. Contreras, T. Nakada and H. W. Schock, *Thin Solid Films* **480**, 273 (2005).

[81] M. Topic, F. Smole and J. Furlan, *Sol Energ Mat Sol C* **49**, 311 (1997).

[82] P. Zabierowski, U. Rau and M. Igalson, *Thin Solid Films* **387**, 147 (2001).

[83] M. Igalson, M. Bodegard, L. Stolt and A. Jasenek, *Thin Solid Films* **431**, 153 (2003).

[84] M. Igalson and C. Platzer-Bjorkman, *Sol Energ Mat Sol C* **84**, 93 (2004).

[85] S.M. Sze, *Physics of Semiconductor devices*: John Wiley&Sons, (1981).

[86] A.Kanevce, M. Gloeckler, A. O. Pudov and and J.R. Sites, in *Mat. Res. Soc.*, **865**. San Francisco, CA, (2005), p. 221.

[87] A. O. Pudov, *PhD Thesis*, Colorado State University (2005) p.22, URL: http://www.physics.colostate.edu/groups/photovoltaic/PDFs/A.Pudov_Thesis_Twoside_Online.pdf

[88] T. Minemoto, Y. Hashimoto, W. Shams-Kolahi, T. Satoh, T. Negami, H. Takakura and Y. Hamakawa, *Sol Energ Mat Sol C* **75**, 121 (2003).

[89] T. Minemoto, Y. Hashimoto, T. Satoh, T. Negami, H. Takakura and Y. Hamakawa, *J Appl Phys* **89**, 8327 (2001).

[90] Falah Hasoon, private comunication

[91] R. N. Bhattacharya, M. A. Contreras and G. Teeter, *Jpn J Appl Phys 2* **43**, L1475 (2004).

[92] A. Pudov, J. Sites and T. Nakada, *Jpn J Appl Phys 2* **41**, L672 (2002).